Journal of Geodynamics 113 (2018) 13–31

Contents lists available at ScienceDirect

Journal of Geodynamics

journal homepage: www.elsevier.com/locate/jog

Late Eocene volcanism in North Patagonia (42°30′–43°S): Arc resumption after a stage of within-plate magmatism

Lucía Fernández Paz[a,*], Vanesa D. Litvak[a], Andrés Echaurren[a], Sofía B. Iannelli[a], Alfonso Encinas[b], Andrés Folguera[a], Víctor Valencia[c]

[a] Universidad de Buenos Aires, Consejo Nacional de Investigaciones Científicas y Técnicas. Instituto de Estudios Andinos "Don Pablo Groeber" (IDEAN), Facultad de Ciencias Exactas y Naturales, Intendente Güiraldes 2160, Ciudad Universitaria, C1428EHA, Buenos Aires Argentina
[b] Departamento de Ciencias de la Tierra, Universidad de Concepción, Casilla 160-C, Concepción, Chile
[c] School of the Environment, Washington State University, Pullman, WA 99164, USA

ARTICLE INFO

Keywords:
Patagonian andes
Arc volcanism
Geochemistry
Decompression melting
Extensional tectonics

ABSTRACT

Mid-Cenozoic widespread arc magmatism in North Patagonia extends from the forearc to the retroarc zones, representing an anomalous large volume when compared to the present-day arc zone and even other past arc configurations. It represents a crucial stage in Andean arc evolution as was developed after a period of arc waning and within plate magmatism. Controversies exist regarding the origin of these volcanic sequences, with scarce integrated field, geochemical and geochronological analyses. We focused our study on the El Maitén Belt, located in the present-day retroarc zone, particularly on a poorly studied section corresponding to the southern outcrops of this volcanic belt. This volcanism consists of basaltic and andesitic lava flows and interbedded pyroclastic deposits, whose emplacement was controlled by extensional tectonics as indicated by the occurrence of wedge-like strata associated with normal faults. A U-Pb age on the basal part of this section shows that magmatic activity started by 37 Ma, earlier than previous studies that considered this volcanism as Oligocene. Geochemically, these rocks are part of the subalkaline and particularly tholeiitic series. All samples show trace element enrichments, depletions and ratios characteristic of arc magmas, though fluids and sediment imprint seem limited. On these bases, we propose decompression melting as the main process associated with the genesis of this volcanism. Therefore, this magmatic association constrained to the late Eocene represents the earliest evidence of arc volcanism in the Patagonian Andes, under an extensional regime, after a Paleogene waning of arc activity.

1. Introduction

The development of a magmatic arc represents the product of subduction, driven by dehydration reactions on the downgoing oceanic slab (Gill, 1981). Arc-related magmatism reflects variations in the composition of the mantle source, the degree of melting, and the nature and amount of subducted material involved during its genesis (e.g., Hofmann et al., 1986; Jacques et al., 2013; Wehrmann et al., 2014). Additionally, the interaction between the continental upper plate and the subducting oceanic slab plays an important role in magmatic arc development (Ducea et al., 2015b), being influenced by changes in plate convergence, absolute motion of the upper plate, geometry of the slab, and the age of the subducted slab among other controls (e.g., Cross and Pilger, 1982; Heuret and Lallemand, 2005; Horton and Fuentes, 2016; Lee et al., 2009; Silver, 1998).

Arc development is controlled by the position of the magmatic locus relative to the trench, which can change, along with magma production rates, as a function of plate dynamics (e.g., Chapman et al., 2017; DeCelles et al., 2009; Karlstrom et al., 2014). Two end-members of this situation can be represented by a shallow subduction setting and a slab rollback scenario. In the first case, magmatism migrates toward the retroarc zone, governed by a compressive regime on the upper plate (e.g., Cross and Pilger, 1982; Ducea et al., 2015a; Folguera and Ramos, 2011). Contrastingly in the case of slab rollback, oceanward retreat and steepening of the slab moves the magmatic locus toward the trench, under an extensional regime in association with the development of intra- and- retroarc basins (e.g., Encinas et al., 2016; Jordan et al., 2001; Rosenbaum and Lister, 2004). Under certain conditions, subduction systems can experience a waning in arc activity. These periods are considered a key point in the evolution of subduction margins as

* Corresponding author.
E-mail addresses: luciafp@gl.fcen.uba.ar (L. Fernández Paz), vane@gl.fcen.uba.ar (V.D. Litvak), andresechaurren@gmail.com (A. Echaurren), iannelli@gl.fcen.uba.ar (S.B. Iannelli), aencinas@udec.cl (A. Encinas), andresfolguera2@yahoo.com.ar (A. Folguera), vicvalencia1@gmail.com (V. Valencia).

https://doi.org/10.1016/j.jog.2017.11.005
Received 17 July 2017; Received in revised form 23 October 2017; Accepted 7 November 2017
Available online 08 November 2017
0264-3707/

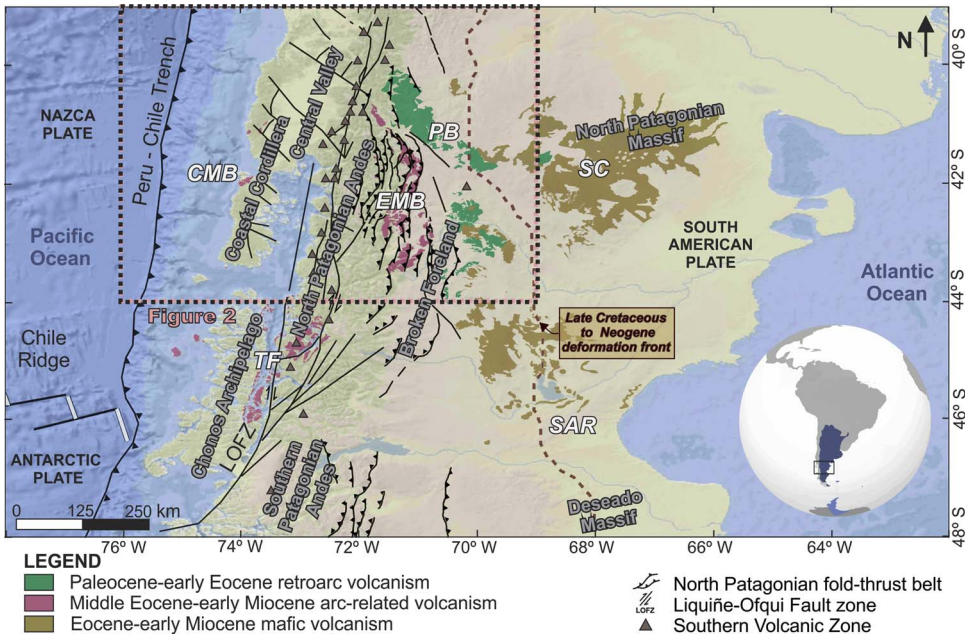

Fig. 1. Tectonic setting of the North Patagonian fold-thrust belt and easternmost limit of the Andean deformation (Echaurren et al., 2016; Gianni et al., 2015; Lavenu and Cembrano, 1999; Muñoz et al., 2000; Orts et al., 2012). The main morphostructural units that constitute the North Patagonian Andean margin are the Coastal Cordillera, Central Valley, North Patagonian Andes, and the broken foreland area. Triangles represent the active volcanic front (Lopez-Escobar et al., 1995), showing a close spatial relationship with the Liquiñe-Ofqui Fault Zone. CMB: Coastal Magmatic Belt; TF: Traiguén Formation; EMB: El Maitén Belt; PB: Pilcaniyeu Belt; SC: Somuncura province; SAR: Paleogene mafic volcanism in Sarmiento Region.

they frequently obey to particular events such as the development of shallow subduction settings and/or collision of mid ocean spreading centers (Cole and Stewart, 2009; Folguera and Ramos, 2011; and references therein). Even though several works illustrated the onset of arc magmatism after arc-waning stages (e.g., Ferrari et al., 2012; Lee et al., 2009; Rossel et al., 2013), common patterns and insights on the petrologic and geochemical characteristics of the initial arc-related magmas are barely addressed in Andean evolution.

In order to evaluate arc characteristics through a period of arc resumption; we studied a particular sector in the North Patagonian Andes where arc activity registered a waning (gap) in early Paleogene times (Fig. 1). During the Late Cretaceous the magmatic locus had migrated toward the retroarc zone, coincidentally with a compressive regime (Echaurren et al., 2016), while an extensional regime was established later in the Paleogene coinciding with the mentioned gap in arc activity (Aragón et al., 2013, 2011b; Pankhurst et al., 1999). This last setting was characterized by Paleocene–early Eocene bimodal volcanism in the former retroarc zone (Pilcaniyeu Belt; Rapela et al., 1988, 1984) (Fig. 1), interpreted as a within-plate magmatic association, promoted by a slab detachment after the subduction of the Aluk-Farallón mid-ocean ridge (Aragón et al., 2013, 2011b). Then, late Oligocene–early Miocene arc-related volcanism was registered in the eastern North Patagonian Andes, as part of the El Maitén Belt (Rapela et al., 1988), although the exact timing, involved processes in magma genesis and tectonic setting of this arc resumption are still discussed (Fig. 1). This arc stage would have been associated with the rollback of the subducted Farallón and Nazca plates that promoted invigorated asthenospheric circulation, giving as a consequence a mixture of slab-modified and pristine magma sources, coeval with a migration of arc magmatism toward the trench (Encinas et al., 2016; Jordan et al., 2001; Muñoz et al., 2000).

This study is focused on the Rivadavia range (Fig. 2), where arc-related series are exposed at the southern part of the El Maitén Belt, which had been primarily assigned to the late Oligocene (Rapela et al., 1988). In order to determine a coherent framework for the evolution of the Paleogene magmatism in the North Patagonian Andes, we carried out field, geochemical and geochronological studies comparing our results with other spatially and temporally related magmatic units. Then, our findings indicate that this volcanic activity marks the resumption of arc magmatism under extensional conditions during the upper Eocene, after a protracted gap in arc activity and within-plate magmatism in Patagonia.

2. Geological setting

The study area is located in the eastern slope of the North Patagonian Andes, in the transition zone with a series of ~N-striking ranges to the east referred to as the Patagonian broken foreland (e.g., Bilmes et al., 2013; Echaurren et al., 2016; Orts et al., 2012) (Fig. 1).

These broken foreland ranges are locally cored by basement units comprising Upper Paleozoic igneous and metamorphic rocks (Caminos and Llambías, 1984; Volkheimer, 1964), intruded by an Early Jurassic NW-striking plutonic belt known as the Subcordilleran Batholith (Gordon and Ort, 1993; Rapela et al.,2005). To the west, the axial part of the North Patagonian Andes is formed by the Mid Jurassic-Cretaceous North Patagonian Batholith that includes a series of calc-alkaline granitoid suites (Aragón et al., 2011a; Castro et al., 2011; González Díaz, 1979; González Díaz and Lizuaín, 1984; Pankhurst et al., 1999). Volcanic counterparts (Jurassic Lago La Plata Formation and mid-Cretaceous Divisadero Group) are spread out toward the east reaching the Patagonian broken foreland (Echaurren et al., 2017; Haller and Lapido, 1982).

Cenozoic units are exposed from the North Patagonian Andes to the Patagonian broken foreland, including volcano-sedimentary sequences with different geochemical imprints (Rapela et al., 1988; Figs. 1 and 2). Paleocene-Eocene magmatism is represented by the 60–42 Ma Huitrera Formation, known in the geological literature as the Pilcaniyeu Belt, which extends between 40° and 44°S in the broken foreland zone (Feruglio, 1949; Ramos, 1982; Rapela et al., 1988). This belt comprises a bimodal association of volcanic rocks interbedded with continental deposits (Rapela et al., 1988, 1984, 1983). The volcanic rocks consist of calc-alkaline ignimbrites at the basal part of this unit and within-plate alkali basalts and tholeiitic basalts-trachytes at the upper part (Aragón et al., 2013, 2011b). This sequence was genetically interpreted as an ignimbrite flare up with a final basaltic stage due to the development of a slab window (Aragón et al., 2013).

Oligocene–early Miocene volcanism (32–20 Ma) is included in the Ventana Formation (González Bonorino, 1973). This volcanism forms part of the El Maitén Belt (Rapela et al., 1988), which extends in a N-S direction between 40° and 43°S, to the west of the Pilcaniyeu Belt and toward the cordilleran axis. The El Maitén Belt comprises volcano-sedimentary sequences that consist of basaltic and andesitic lavas and

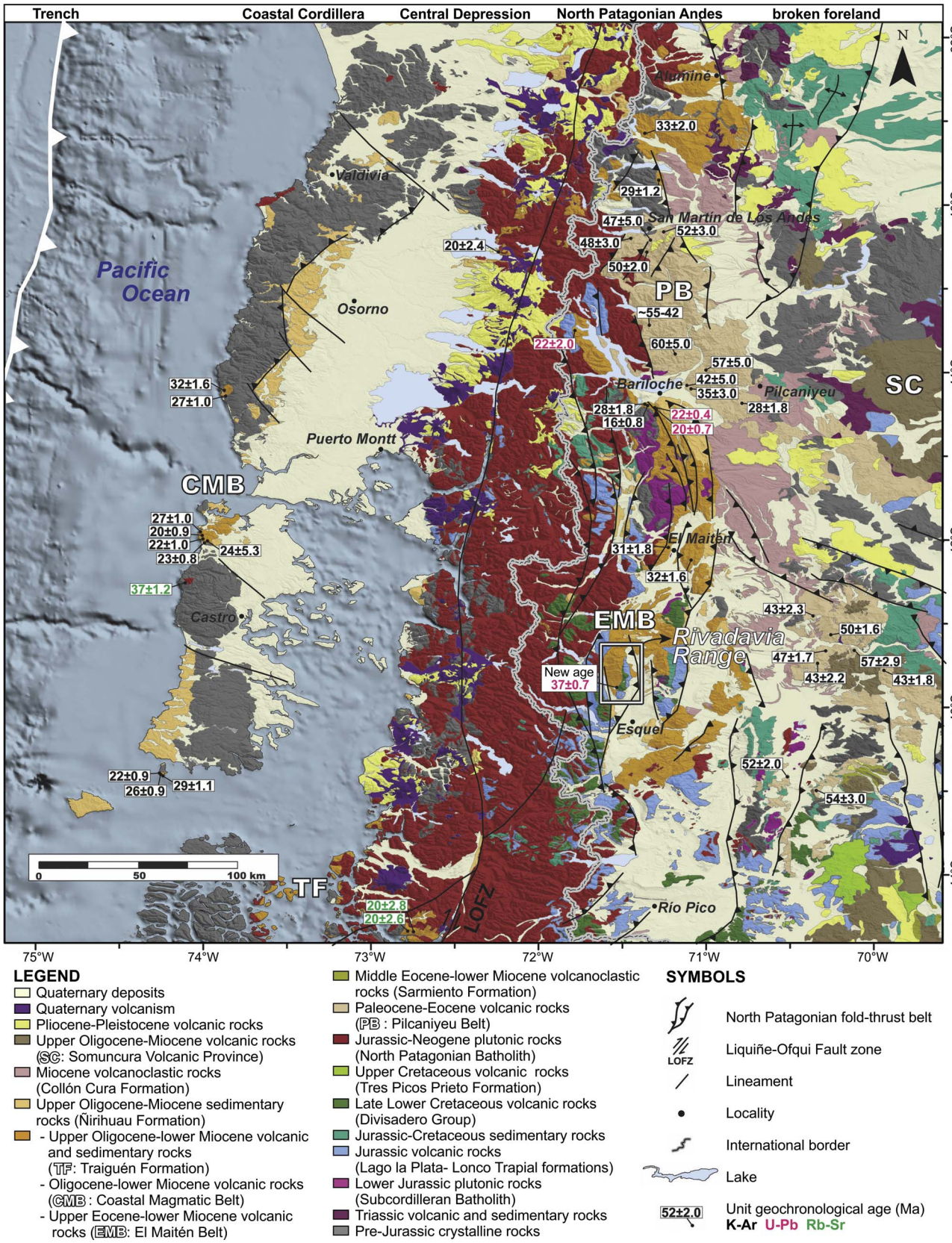

Fig. 2. Geological map of northern Patagonia from Sernageomin (2003), González (1994) and Lizuain et al. (1995), with the Paleogene-lower Neogene volcano-sedimentary sequences highlighted: CMB, Coastal Magmatic Belt (37?; 29–18 Ma); EMB, El Maitén Belt (37–20 Ma); PB, Pilcaniyeu Belt (60–42 Ma); TF, Traiguén Formation (32?, 26–20 Ma); SC, Somuncura province (29–16 Ma). Radiometric ages are from Aragón et al. (2011a), Bechis et al. (2014), Encinas et al. (2014), González Bonorino and González Bonorino (1978), González Díaz (1979), Henríquez Ascencio (2016), Iannelli et al. (2017b), Kay et al. (2007), Lizuain and Viera (2010), Mazzoni et al. (1991), Muñoz et al. (2000), Rabassa (1974), Ramos et al. (2014), Rapela et al. (1988, 1983), and Turner (1982). Note the square denoting the Rivadavia range location.

minor pyroclastic rocks, interbedded with marine deposits at the upper part of this unit (Bechis et al., 2014; Dalla Salla et al., 1981; González Bonorino, 1973; Ramos, 1982; Rapela et al., 1988). These volcanic rocks were geochemically described as calc-alkaline, with a change to tholeiitic compositions toward the upper part of the unit (Iannelli et al., 2017b; Litvak et al., 2014; Rapela et al., 1988, 1983). It was also proposed that this volcanic belt evolved in the context of progressive crustal thinning related to a regional extensional stage that favored the incursion of a marine transgression during the earliest Miocene (Bechis et al., 2014; Rapela et al., 1988). Northern outcrops of this unit near Bariloche city (40°S) show middle/upper Paleocene to lower Miocene ages, based on Rb-Sr and K-Ar methods (González Bonorino, 1973; González Bonorino and González Bonorino, 1978; González Díaz, 1979; Rapela et al., 1988, 1983), and more recent lower Miocene U-Pb ages (Aragón et al., 2011a; Bechis et al., 2014; Fig. 2). Southern outcrops between the localities of El Maitén and Esquel (42°–43°S) show that the earliest magmatic activity could be assigned to the Eocene on the basis of its fossil flora (Sepúlveda, 1980), with also scarce K/Ar Eocene and Oligocene ages (Cazau et al., 1989; Lizuain and Viera, 2010; Rapela et al., 1988) (Fig. 2). Despite the limited consensus regarding the age of El Maitén Belt, it is presently assigned to the Oligocene-lower Miocene, considering reliable K-Ar ages and the new U-Pb ones. At these latitudes (40°–43°S), partly contemporaneous volcanic activity is registered in the Coastal Cordillera, referred to as the Coastal Magmatic Belt (~29–18 Ma), composed of basaltic to dacitic lava flows (Muñoz et al., 2000); and to the south in the Chonos Archipelago (~45° S) as pillow basalts and tuffs of the Traiguén Formation (~26–23 Ma) that were erupted in association with an extensional regime (Encinas et al., 2016; Hervé et al., 1995; Silva, 2003). On the foreland zone, contemporaneous volcanism includes a broad mafic plateau, known as the Somuncura province (~29–16 Ma), which was associated with a short asthenospheric anomaly (Kay et al., 2007).

The Oligocene volcanic sequences are overlain by the Ñirihuau (22–16 Ma) and Collón Curá (16–10 Ma) formations, which represent the main infill of the Ñirihuau basin (Bechis et al., 2014; Cazau et al., 1989; Giacosa et al., 2005; Rabassa, 1978; Spalletti, 1983; Yrigoyen, 1969). It was proposed that extensional conditions may have controlled the deposition of the basal part of the Ñirihuau Formation, while the middle and upper parts of this unit and the younger Collón Curá Formation represent synorogenic deposits, associated with the last orogenic uplift and contraction that affected the North Patagonian Andes (Bechis et al., 2014; Echaurren et al., 2016; Orts et al., 2012).

After protracted quiescence in arc-related activity along the Andean axis, the North Patagonian Batholith resumes its magmatic activity in the early Miocene (20 Ma), extending to the Pliocene, localized along the dextral-transpressive Liquiñe-Ofqui Fault Zone (LOFZ) (Fig. 2) (Pankhurst et al., 1999). Recent arc volcanism included in the Southern Volcanic Zone (SVZ), and particularly at the studied latitudes in the South Southern Volcanic Zone (SSVZ), is characterized by highly active centers associated with the LOFZ (e.g., Amigo et al., 2013; Lopez-Escobar et al., 1995; Watt et al., 2011).

3. Geology of the Eocene El Maitén Belt in the Rivadavia range

Sampling and lithofacial analyses of El Maitén Belt volcanic rocks were carried out at the southwestern slope of the Rivadavia range, a ~N to NNW-striking highly asymmetric double-vergent anticline. The western flank of the anticline exposes the volcanic rocks of the El Maitén Belt, while the eastern slope comprises volcano-sedimentary sequences of the Lago la Plata Formation and the Divisadero Group in the core of the anticline (Viera and Hughes, 1999) (Fig. 3).

Volcanic rocks of El Maitén Belt mainly consist in basaltic and andesitic lava flows with interbedded pyroclastic deposits; unconformably covering Mesozoic rocks (Figs. 3 and 4). These constitute a NW-striking section with variable SW dipping horizons. Two high angle E/SE-dipping reverse faults and an associated anticline were recognized in the SE sector, which structurally control the distribution of the volcanic facies (Fig. 3). The southern reverse fault is associated with an asymmetric anticline with a nearly subhorizontal eastern flank and a subvertical western flank. The increasing thickness of the different volcanic units toward the fault plane indicates normal faulting contemporaneous with the emplacement of the volcanic sequence (Echaurren et al., 2016) (Fig. 5).

We defined two lithological domains controlled by the cited NE-trending thrusts: a south-east domain (SED) and a north-west domain (NWD) (Fig. 3). The major lithofacial variation was recognized in the SED, where thicker units from the lower and middle volcanic section crop out including five facies. The NWD comprises the three facies of the upper section, characterized by monolithological outcrops with lower thicknesses (Figs. 3 and 4). A representative vertical section of the volcanic sequence includes the eight defined lithological facies (Fig. 4a), from base to top the succession includes: basaltic andesites, crystalolithic tuffs, fine grained basalts, vesicular basalts, volcanic breccias 1, volcanic breccias 2, aphanitic basalts and columnar andesites. The petrographic features of these rocks are described in Table 1.

The SED consists of a folded sequence that represents the major thickness of the profile (Figs. 3–5). The lower part of the sequence is composed of the basaltic andesites facies (sample RV08; Fig. 4b). This facies consists of 90 m of porphyritic rocks with columnar disjunction, characterized by interstitial quartz and alkali feldspar in granophyric texture. Above, the crystalolithic tuffs facies (sample LS23) extends as a thin horizon (~36 m thick) with a wide lateral continuity (Fig. 3). These light brown and partially stratified pyroclastic rocks (Fig. 5) contain a high percentage of volcanic lithics (45%) and crystal fragments (35%), with minor amounts of pumice and volcanic shards (20%). Microscopically, shards preserve triaxone shapes, while pumices are partially deformed and form occasionally a pseudomatrix.

A thick succession (~170 m thick) of fine grained basalts continues up in the profile, with interbedded levels of vesicular basalts and volcanic breccias (Fig. 4c–f). Fine grained basalts facies consist of 101 m of greenish gray basalts with an intense subhorizontal jointing, whose main feature is the decrease in grain size to the top of the level (samples LS25, LS17, LS07, and LS10). These rocks have aphyric to microporphyritic textures with plagioclase, clinopyroxene and opaque minerals. Groundmass is mainly intersertal to intergranular, with plagioclase as the main phenocryst in the more porphyritic varieties. However, olivine phenocrysts are present at the base of this succession, where ophitic textures are more common. The vesicular basalt facies corresponds to 63 m of gray basalts (sample LS12a), with similar petrographical characteristics as the fine grained basalts, but with a remarkable presence of vesicles (25%), some of them filled with calcite. The interbedded volcanic breccias consist of 5 m of reddish brecciated rocks (sample LS09, volcanic breccias 1 facies) with porphyritic basaltic autoclasts immersed in a volcanic groundmass of similar composition. Some of these autoclasts have clear limits with the matrix, while others have transitional passages, showing their plastic stage at the moment of the incorporation to the lava flow.

The uppermost facies of the profile crop out in the NWD. The first level corresponds to 5.8 m of volcanic breccias (sample LS31, volcanic breccias 2 facies; Fig. 4g) with microporphyritic basaltic autoclasts of 2–20 mm in size, within a matrix of the same composition. Above these rocks, the aphanitic basalt facies comprises 15 m of aphanitic grayish rocks (samples LS30b and LS35b; Fig. 4h and i), which grade from aphyric to microporphyritic textures with plagioclase, clinopyroxene, orthopyroxene and opaque minerals. Finally, the columnar andesites facies is primarily represented by andesitic lava flows of 2 m of thickness exposed toward the top of the profile (sample LS04), and a minor intrusive body (sample LS08), both with a characteristic columnar disjunction (Fig. 4a and j). This facies comprises dark gray porphyritic andesites with plagioclase and orthopyroxene phenocrysts within a glassy groundmass.

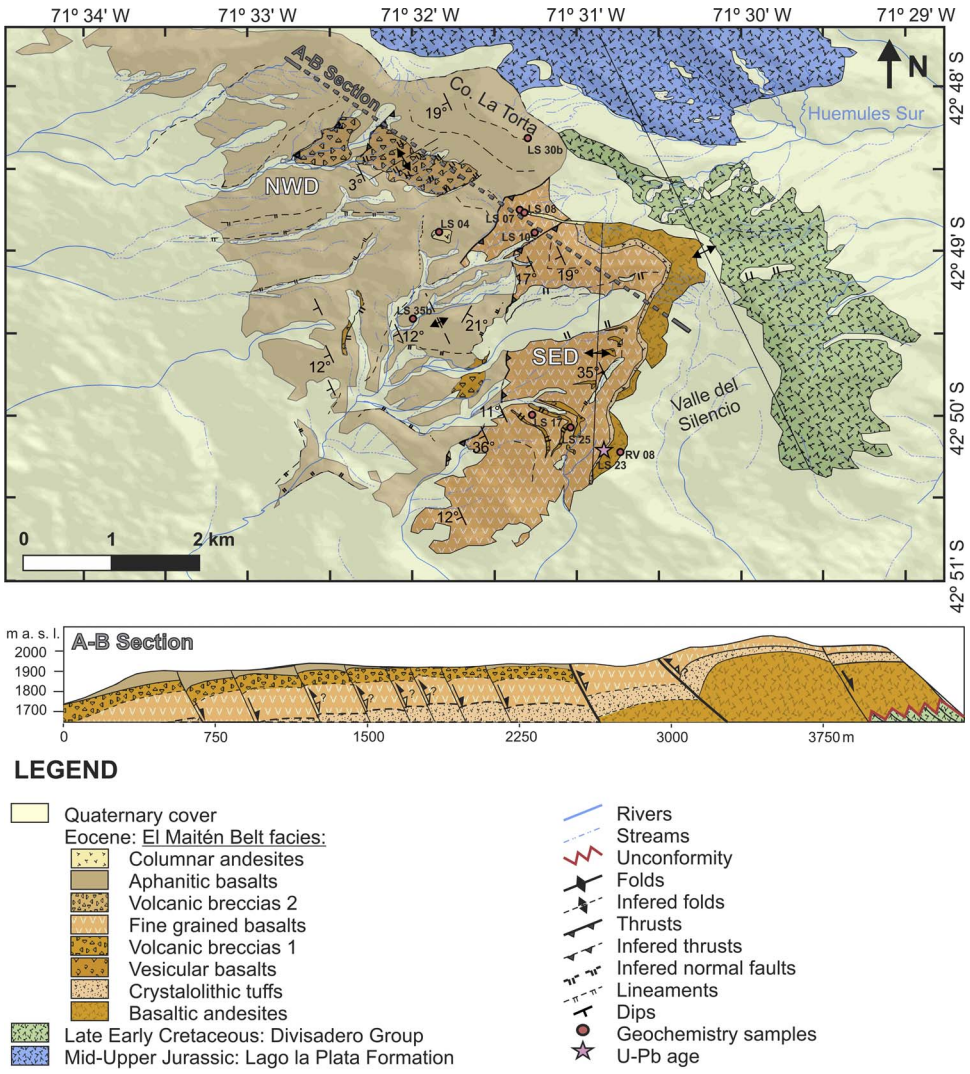

Fig. 3. Geological map of the study area. El Maitén Belt volcanic rocks outcrop in the western slope of the Rivadavia range, showing eight different lithofacies. The A-B section shows the structural control in the emplacement of volcanic sequences as a series of normal faults, some of them partially inverted.

4. Analytical results

4.1. Sampling and methodology

Geochronology analysis was performed through U-Pb Laser Ablation Inductively Coupled Plasma Mass Spectrometry (LA-ICP-MS) on zircons from a crystalolithic tuff from the lower levels of the El Maitén Belt section studied in the Rivadavia range (Sample LS23; see Supplementary Material A for zircon data). Heavy mineral concentrates of the < 350 μm fraction were separated using traditional techniques at ZirChron LLC. Zircons from the non-magnetic fraction were mounted in epoxy and slightly ground and polished to expose the surface for laser ablation analyses. LA-ICP-MS U-Pb analyses were conducted at Washington State University prior to cathodoluminescence (CL) imaging using a New Wave Nd: YAG UV 213-nm laser coupled to a Thermo Finnigan Element 2 single collector, double-focusing, magnetic sector ICP-MS. Operating procedures and parameters are a modification of Chang et al. (2006). Laser spot size and repetition rate were 30 nm and 10 Hz, respectively. He and Ar carrier gases delivered the sample aerosol to the plasma. Each analysis consisted of a short blank analysis followed by 250 sweeps through masses 204, 206, 207, 208, 232, 235, and 238, taking approximately 30 s. Time-independent fractionation was corrected by normalizing U/Pb and Pb/Pb ratios of the unknowns to the zircon standards (Chang et al., 2006). For this study, two zircon standards were used: Peixe, with an age of 564 Ma (Dickinson and Gehrels, 2003), and FC-1, with an age of 1099 Ma (Paces and Miller, 1993). Uranium-lead age was calculated using Isoplot (Ludwig, 2003). The final ages include systematic and analytical errors, which are around 2%.

Geochemical analyses were performed on nine fresh samples, selected for their well-defined stratigraphic relationships, representatives of the lithological facies described in the Rivadavia range (Tables 1 and 2, Fig. 4). Samples for geochemical analyses were prepared and analyzed at the Activation Laboratories of Ancaster, Canada: major, trace and rare earth elements were measured by total fusion and inductively coupled plasma mass spectrometry (FUS-ICP-MS). According to the laboratory procedures (http://www.actlabs.com), unaltered rock fragments were crushed until 90% were < 2 mm. A 250 g split was then pulverized with a mild steel mill until 95% passed through a sieve with a mesh of 105 μm. Samples were prepared and analyzed in a batch system, where they were mixed with a flux of lithium metaborate and lithium tetraborate. The molten melt was immediately poured into a solution of 5% nitric acid containing an internal standard, and was mixed continuously until completely dissolved (~30 min). The samples were run for major oxides and selected trace elements on a Varian Vista 735 ICP-OES. In trace element analysis, fused samples were diluted and analyzed by Perkin Elmer Sciex ELAN 6000. The standards used were NIST-694, DNC-1, W-2a, SY-4 and BIR-1a for major elements and trace elements, plus, LKSD-3, TDB-1, CTA-AC-1, NCS-DC86312, NCS-DC70009, OREAS-100a, OREAS-101a, OREAS-101b and JR-1, also for trace elements (see Supplementary Material B for quality controls). The detection limit for the major oxides is 0.01 wt.%, except for MnO and

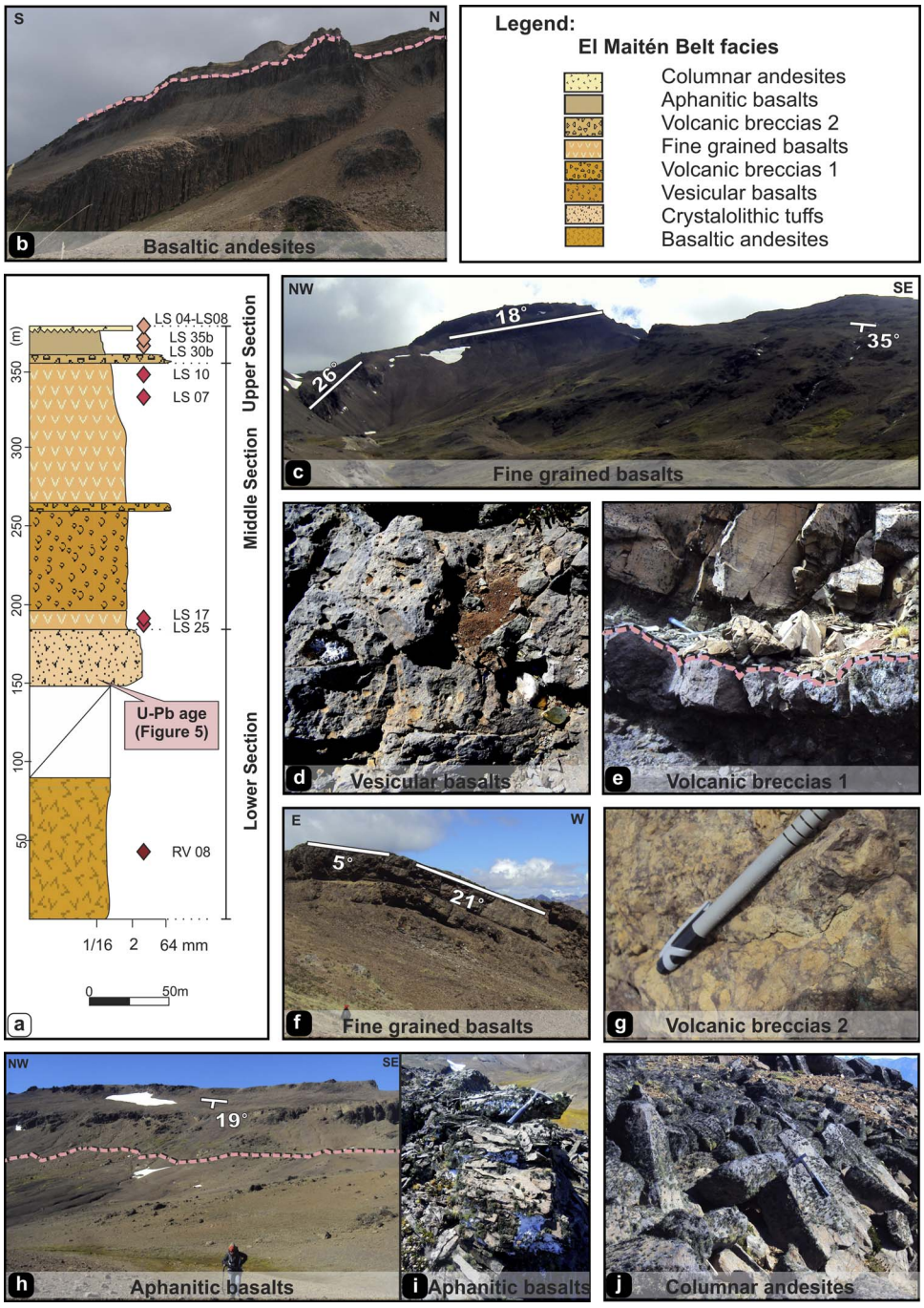

Fig. 4. El Maitén Belt volcanic and volcanoclastic rocks. (a) Representative section of El Maitén Belt volcanism in Rivadavia range. (b) Basaltic andesites exposures with columnar disjuntion, in contact with crystalolithic tuffs facies. (c) Lower section of fine grained basalts facies dipping to SW. (d) Detail of vesicular basalts facies. (e) Irregular contact between reddish volcanic breccias 1 and fine grained basalts above. (f) Upper section of fine grained basalts facies dipping between 5°W and 21°W. (g) Detail of volcanic breccias 2f acies whit clasts of irregular shapes. (h) Contact between aphanitic basalt facies that covers the volcanic breccias 2 facies, both dipping to the SW. (i) Detail of the aphanitic basalt outcrops with their characteristic subhorizontal jointing. (j) Columnar andesites facies cropping out with their typical disjuntion.

TiO_2, which is 0.001 wt.%. For most of the trace elements, the detection limit is 0.01 ppm, with the exception of Sr (2); Rb, Sc, Co, Ga, Zr (1); Ba (3); Pb (5); Zn (30); Cu (10); Th, La, Ce, Nd (0.05); Nb (0.2); Hf (0.1); Y (0.5); Cr, Ni (20); Eu, Tm (0.005) and Lu (0.002).

4.2. U-Pb geochronology of Rivadavia range sequences

The U-Pb geochronological analysis was carried out on a crystalolithic tuff (crystalolithic tuff facies) located near the base of the sequence (Sample LS23; Figs. 4 and 5). Results of the 95 analyzed zircons yielded ages that overlap within the error, suggesting a single source. Th/U ratios for the analyzed zircons are > 0.1, which correspond to a typical igneous origin (Rubatto, 2002). Analyses provide a $^{206}Pb/^{238}U$ mean age of 37.0 +0.7 −0.5 Ma (2 sigma, Fig. 5), which was calculated from a group of 58 zircons with 95% of confidence and ^{207}Pb corrected. A small number of zircons (n = 5) shows ages between Jurassic to Cretaceous, representing the underlying Mesozoic volcanic sources (Divisadero Group and Lago la Plata Formation); while another group (n = 7) yields ages between 47.2 and 63.4 Ma, probably related to the Paleocene-Eocene magmatism cropping out to the west (Pilcaniyeu Belt).

This new determination indicates an upper Eocene age for the studied sequences, and corroborates previous paleontological determinations of an Eocene age for similar outcrops exposed in the northern area of the Rivadavia range (Sepúlveda, 1980).

4.3. Geochemistry of El Maitén Belt volcanism at the Rivadavia range

4.3.1. Major elements

Basaltic to andesitic lava flows comprise a SiO_2 content from 49.64

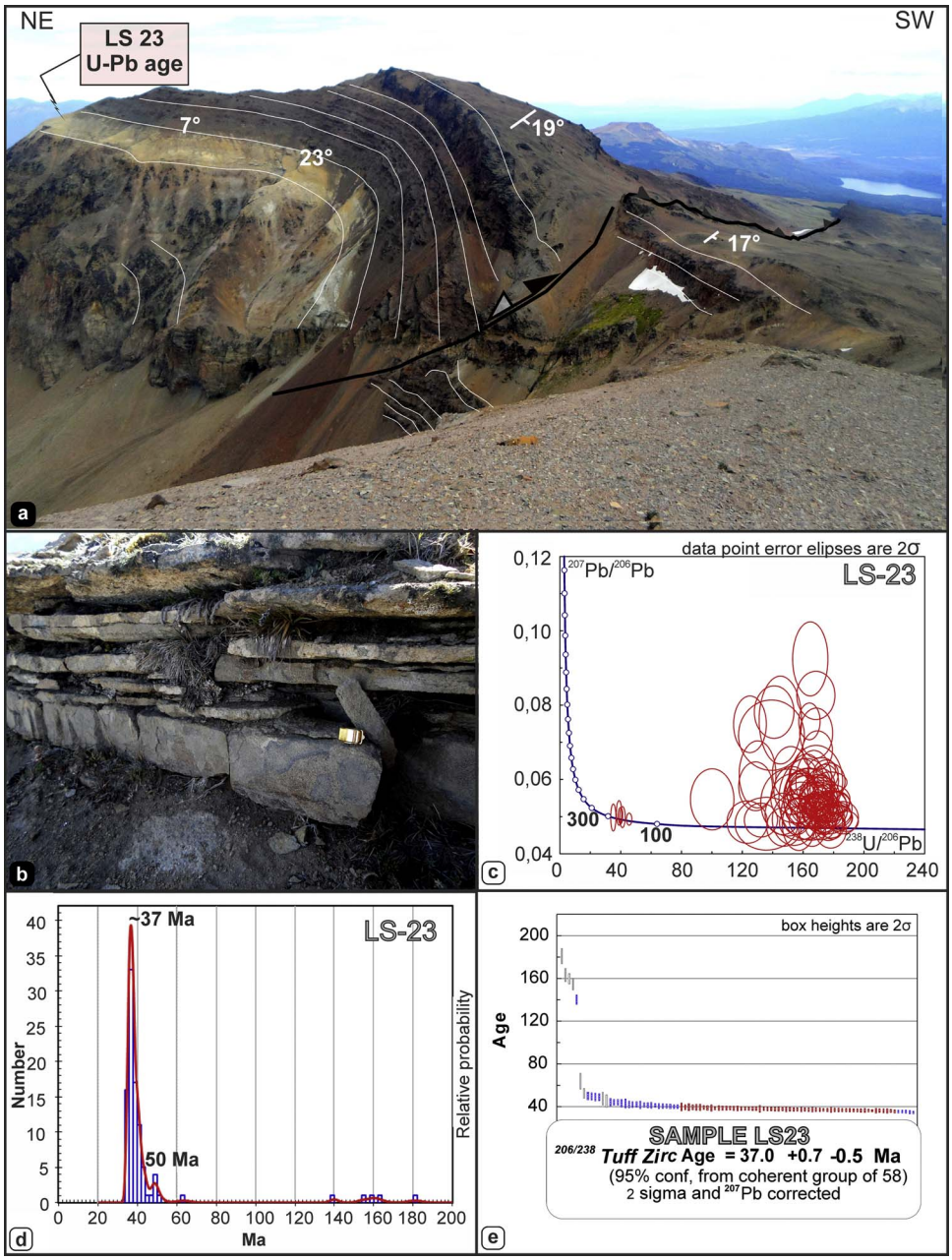

Fig. 5. (a) Outcrops of El Maitén Belt facies recognized in the SED of the studied area; note the increase in thickness of the different volcanic levels toward a partially inverted normal fault. (b) Detail of the crystalolithic tuffs facies outcrops with their characteristic subhorizontal stratification. (c) Concordia diagram of LA–ICP–MS U–Pb age for sample LS23 from Rivadavia range. (d) Probability density functions of detrital zircon ages. A main probability of ~37 Ma age was obtained for El Maitén Belt sample, with minor peaks in 50, 140, 160 and 180 Ma mainly represented in the region by the Pilcaniyeu Belt, the Divisadero Group and the Lago La Plata Formation. (e) Resulted ages calculated from a group of 58 grains, ^{207}Pb corrected. All uncertainties are 2 sigma; systematic, analytical and propagation errors are included.

to 66.02 wt.%, increasing gradually from the base to the top of the sequence. The only exception to this trend is the sample RV08 from the lower section (64.32 wt.%), which shows high silica content due to the presence of interstitial quartz and alkali-feldspar (see Table 1). Based in the total alkalis vs. silica classification (Fig. 6), samples are basaltic andesites, andesites and dacites representatives of the subalkaline series. This geochemical classification does not coincide with the petrographical characterization, a discrepancy that is justified by the high percentage of interstitial volcanic glass (see Table 1). The rocks show FeOt/MgO ratios comparable with tholeiitic series and K_2O contents from 0.76 to 2.7 wt.% (corresponding to medium-K series); an exception to this is the dyke of the upper section which plots in the calc-alkaline field (Fig. 6).

Harker diagrams (Fig. 7) show negative correlation of Al_2O_3, MgO, CaO and TiO_2 oxides with SiO_2, consistent with the fractionation of calcic plagioclase, olivine, clinopyroxene and ilmenite or titanomagnetite (decreasing CaO, MgO and TiO_2), while positive correlations of Na_2O and K_2O would indicate no alkali feldspar fractionation. Fe_2O_3 and P_2O_5 have positive correlations at early crystallization stages (samples with < 55 wt.% of SiO_2) and negative correlations in more evolved samples (SiO_2 > 55 wt.%), common in tholeiitic series where magnesium olivines fractionated first, while clinopyroxene is dominantly fractionated in later crystallizing phases. Apatite fractionation in more evolved samples also explains the inflexion in P_2O_5 trend.

4.3.2. Trace elements

According to compatible trace elements content, the more primitive signature is shown by the basalts stratigraphically located at the base of the middle section (fine grained basalts, samples LS17 and LS25), with the highest Ni, Co, Cr, and Mg# values (Ni = 50–80 ppm, Cr = 30–160 ppm, Co = 21–37 ppm and Mg# = 42–56). Representative trace elements content plotted against silica content (Fig. 7) show increasing Rb, Ba, Th and Zr with increasing differentiation, which indicates that none of these elements were incorporated in the crystallizing phase. A slightly negative correlation of Sr with increasing SiO2 content indicates fractionation of plagioclase;

Table 1
Petrographic features of the defined facies of the El Maitén Belt in the western slope of Rivadavia range. Underlined rows correspond to volcanoclastic features.

Coordinates	Sample	Facies	Composition	Phenocrysts // Clasts						Groundmass				Observations
				%	Texture	%	Mineral	Size (mm)	Shape	%	Texture	%	Mineral	
42°48'53"S; 71°31'52"W	LS04*	Columnar andesites	Andesite	40	Porphyritic	40 60 –	Orthopyroxene Plagioclase –	0.2–1.5 1.6–2.7 –	Subhedral Subhedral –	60	Hyalopilitic	50 30 20	Plagioclase Orthopyroxene Opaque	Two types of glass: a reddish and fresh one, and a gray and moderate clay-altered one.
42°48'45"S; 71°31'21"W	LS08*	Columnar andesites	Andesite	20	Porphyritic	100	Plagioclase	0.8–2.4	Subhedral	80	Hyalopilitic	80 15 5	Plagioclase Opaque Apatite	Brown glass with moderate clay alteration. Amygdales (5%) filled with botroidal clays.
42°49'24"S; 71°32'2"W	LS35b*	Aphanitic basalts	Basalt	–	Aphyric	–	–	–	–	100	Intersertal	80 20	Plagioclase Opaque	Fluidal appearance. Interstitial slightly altered glass.
42°48'18"S; 71°31'20"W	LS30b*	Aphanitic basalts	Basalt	5	Micro-Porphyritic	80 10 10 –	Plagioclase Orthopyroxene Clinopyroxene –	0.1-0.2 0.6-0.8 0.5	Subhedral Subhedral Subhedral	95	Felty/ Intersertal	40 25 20 15	Plagioclase Opaque Orthopyroxene Clinopyroxene	Two types of glass: a fresh and uncolored one, and a moderate clay-altered one.
42°48'30"S; 71°31'39"W	LS31	Volcanic breccias 2	Basalt	60	Volcanic Breccia	100	Porphyritic basalt grains	Feb–20	Rounded	40	Porphyritic	100	Basalt grains	Clast are noted for their high oxidation
42°48'44"S; 71°31'23"W	LS07*	Fine grained basalts	Basalt	–	Aphyric	–	–	–	–	100	Intersertal	55 35 10	Plagioclase Clinopyroxene Opaque	Fluidal appearance. Interstitial slightly altered glass.
42°48'53"S; 71°31'17"W	LS10*	Fine grained basalts	Basalt	25	Porphyritic	100	Plagioclase	01–Feb	Euhedral	75	Intersertal	45 40 15	Plagioclase Clinopyroxene Opaque	Interstitial uncolored and slightly altered glass
42°48'53"S; 71°31'17"W	LS09	Volcanic breccias 1	Basalt	40	Volcanic Breccia	100	Porphyritic basalt grains	Feb–20	Rounded	60	Porphyritic	100	Basalt grains	Clast are noted for their high oxidation
42°49'27"S; 71°30'45"W	LS12a	Vesicular basalts	Basalt	20	Porphyritic	80 15 5	Plagioclase Olivine Opaque	1.25-2 0.2-0.3 0.2-0.3	Subhedral Euhedral Subhedral	80	Felty	75 15 10	Plagioclase Clinopyroxene Opaque	25% vesicles and calcite amygdales
42°50'4"S; 71°31'4"W	LS25*	Fine grained basalts	Basalt	10	Micro-Porphyritic	100	Olivine	0.25-1	Anhedral	90	Subophitic	45 35 20	Plagioclase Clinopyroxene Opaque	This unit also includes aphyric varieties
42°49'59"S; 71°31'18"W	LS17*	Fine grained basalts	Basalt	20	Micro-Porphyritic	60 35 5	Plagioclase Olivine Opaque	0.75-3.5 0.25 0.25	Subhedral Euhedral Anhedral	80	Subophitic	50 30 20	Plagioclase Opaque Clinopyroxene	This unit also includes aphyric varieties
42°50'12"S; 71°30'52"W	LS23	Crystalolithic tuffs	Crystalolithic tuffs	90	Clast supported (0.25-0.5 mm)	45 35 20	Lithic fragments Crystal fragments Glass fragments	0.4-0.8 0.12-0.8 0.4-0.8	Subangular Angular Subangular Angular	10	Matrix	100	Volcanic dust (Clay altered)	Vitreous fragments are deformed, forming part of the pseudomatrix. Secondary silica and zeolites appear interstitially as cement
42°50'13"S; 71°30'46"W	RV08*	Basaltic andesites	Basalt	20	Porphyritic	90 10	Plagioclase Clinopyroxene	0.2-0.8 0.3	Subhedral Subhedral	80	Felty	50 15 15 10 10	Plagioclase Clinopyroxene Opaque Quartz Alkali Feldspar	Quartz and alkali feldspar constitute granophyric textures

* Chemically analyzed samples.

Table 2
Geochemical results of the Eocene El Maitén Belt volcanic rocks. Samples location and lithological type are given in Table 1.

Sample	RV08	LS17	LS25	LS10	LS07	LS30B	LS35B	LS08	LS04
Major and minor elements (wt.%)									
SiO_2	64.32	52.85	49.64	54.32	56.79	60.98	64.4	65.86	66.02
Al_2O_3	14.85	16.87	16.78	17.27	16.4	15.92	15.88	14.55	14.79
Fe_2O_3t	5.55	9.9	8.26	9.31	8.16	6.28	5.04	4.72	5.18
MnO	0.098	0.143	0.101	0.198	0.136	0.108	0.08	0.122	0.11
MgO	1.2	4.54	5.43	3.52	2.53	1.64	0.72	1.58	0.86
CaO	2.46	7.74	7.91	6.73	5.67	5.43	3.38	2.18	2.7
Na_2O	4.64	4.01	3.73	4.12	4.07	3.78	4.49	4.51	5.4
K_2O	2.7	0.92	0.76	1.29	1.87	1.99	2.42	2.45	2.01
TiO_2	0.689	1,962	1,921	1,657	1,451	1.19	0.518	0.665	0.671
P_2O_5	0.22	0.4	0.38	0.65	0.55	0.35	0.28	0.21	0.22
LOI	2.17	1.38	3.6	1.03	0.94	1.49	1.65	2.19	2.02
Total	98.89	100.7	98.51	100.1	98.56	99.16	98.85	99.04	100
Trace elements (ppm)									
Sc	10	24	26	19	16	16	5	10	10
V	29	202	190	141	134	139	10	28	27
Cr	< 20	30	160	< 20	20	30	20	20	< 20
Co	7	29	34	21	19	16	6	6	6
Ni	< 20	80	70	50	< 20	< 20	< 20	< 20	< 20
Rb	92	20	12	30	73	88	97	69	112
Sr	182	366	350	379	331	294	296	180	187
Y	48.8	29.1	33.6	36.6	36.8	28.3	34.5	44.4	42.6
Zr	382	210	222	267	269	198	407	364	413
Nb	13.3	3.5	8.6	6	9.2	7.6	8.7	12.2	15.2
Cs	1.8	0.3	0.2	0.7	1.8	3.4	3.3	0.5	4.5
Ba	570	188	132	305	377	383	572	564	619
La	40.4	16.6	16.2	23.8	27.8	23.5	32.8	36.8	35.8
Ce	80.9	39.3	38.5	54.8	61.2	47.7	67.5	76.7	76.3
Pr	10.1	5.37	5.15	7.37	7.99	5.95	8.19	9.04	9.06
Nd	37.8	22.6	22.5	31.3	31.7	23.5	30.7	33	34.5
Sm	8.14	5.52	5.5	7.42	7.06	5.52	6.38	6.91	7.5
Eu	1.95	1.8	1.89	2.39	2.21	1.59	1.86	1.84	1.8
Gd	8.14	5.62	5.82	7.28	7.1	5.57	5.74	6.84	6.98
Tb	1.31	0.9	0.95	1.13	1.15	0.85	0.96	1.15	1.14
Dy	7.88	5.47	5.8	6.97	6.63	4.93	5.59	7.12	6.99
Ho	1.6	1.09	1.15	1.37	1.29	0.95	1.11	1.48	1.4
Er	4.58	3.23	3.31	3.73	3.66	2.65	3.51	4.37	4.08
Tm	0.68	0.463	0.48	0.534	0.525	0.381	0.526	0.668	0.62
Yb	4.59	3.02	3.03	3.55	3.44	2.44	3.61	4.33	4.27
Lu	0.742	0.466	0.483	0.571	0.561	0.359	0.594	0.705	0.675
Hf	8.6	4.2	4.7	4.8	5.9	4.7	8.5	8	9.1
Ta	1.09	0.53	0.64	0.67	0.78	0.71	0.8	1.09	1.07
Pb	14	< 5	< 5	7	10	12	14	14	14
Th	9.25	2.33	1.81	3.67	5.32	6.58	7.03	8.9	9.01
U	2.11	0.53	0.24	0.88	1.38	1.99	1.81	2.08	2.17

whereas the more pronounced decrease of V implies ilmenite and/or titanomagnetite fractionation. A scattered trend is shown in Y vs. SiO_2 diagram, which suggests that fractional crystallization had probably no particular influence on Y content.

Selected trace elements ratios were plotted against silica content in order to discard the effects of fractional crystallization on these ratios, for its later use as tectonic discriminants (Fig. 7). U/Th, Pb/Ce and Ba/Nb do not correlate or correlate weakly with SiO_2 content, and therefore appear to be not significantly influenced by fractional crystallization. However, some anomalous values are seen in Ba/Nb ratios, which are associated with anomalous Nb contents in some samples from the middle section.

Multi-element diagrams are characterized by patterns with slightly Rb, Ba, Th, U, La and Pb enrichment relative to the negative Nb-Ta, Sr-P and Ti anomalies (Fig. 8). Enrichment in these large ion lithophile elements (LILE) relative to the high field strength elements (HFSE) is associated with hydrous fluids driven off subducted oceanic crust into the asthenospheric-mantle source. Particularly, samples with higher silica content (> 55 wt.% SiO_2) show more marked negative anomalies in Nb-Ta, Sr-P and Ti. The depletion in Sr within these samples may be associated with plagioclase fractionation, while P and Ti negative anomalies may occur as a consequence of fractional crystallization of accessory minerals such as apatite and Fe-Ti oxides. A conspicuous feature between basic and intermediate samples is a change in Ba behavior, represented by a negative anomaly in more evolved rocks, possibly as a result of amphibole fractionation.

Rare earth element diagrams show flat patterns with low light REE (LREE) ($(La/Sm)_n$ = 1.86–3.8) and heavy REE (HREE) ($(Sm/Yb)_n$ = 1.73–2.45) ratios, despite silica content (Fig. 8). Samples with < 55 wt.% SiO_2 show slightly positive anomalies (Eu/Eu* = 0.99–1.03), that could reflect plagioclase accumulation (Vukadinovic, 1993). In contrast, intermediate to acid rocks (> 55 wt.% SiO_2) have a small negative Eu anomaly (Eu/Eu* = 0.74–0.96), that accompanied by Sr depletion suggests an incipient plagioclase fractionation.

The analyzed volcanic rocks display an increase in La/Yb (La/Yb = 5.35–9.63) and a decrease in Dy/Yb ratios (Dy/Yb = 2.02–1.55) with increasing silica content (Fig. 9). Comparisons with expected fractionation effects for intermediate rocks indicate that the studied samples respond more to amphibole fractionation than to a magma differentiation trend, with clinopyroxene controlling differentiation (Davidson et al., 2007; Macpherson et al., 2006).

Differences between LILE, HFSE and REE contents can be highlighted with trace elements ratios, which might reflect variable tectonic settings. Studied samples show La/Ta = 25.31–41, Nb/La = 0.2–0.53, Ba/La = 8.15–17.44, Ba/Ta = 206–715 and Ba/Nb = 15.35–65.75 contents. In comparison with typical arc values (La/Ta > 25, Ba/La > 20, Ba/Ta > 500, Ba/Nb > 30 and Nb/La < 0.5), the analyzed samples have La/Ta and Nb/La ratios that resemble arc composition, while Ba/La, Ba/Ta and Ba/Nb show lower ratios (Fig. 10).

5. Discussion

5.1. Geochronological and geochemical constraints on the upper Eocene El Maitén Belt volcanism

The El Maitén Belt was defined as a voluminous volcanic belt developed along the eastern slope of the North Patagonian Andes, in the present-day retroarc zone (40°–43°S, Fig. 2) (Rapela et al., 1988, 1984). Despite its location and big volume within the continental interior, these volcanic sequences were interpreted as indicative of a Paleogene arc activity (Dalla Salla et al., 1981; Rapela et al., 1988, 1984). Temporal constraints, derived mostly on the basis of Rb-Sr and K-Ar ages with limited U-Pb ages, assigned the northern outcrops of this belt to a large time span between upper Paleocene and lower Miocene times. However, the restricted continuity between outcrops and the close spatial association with the older Pilcaniyeu Belt (mainly around ~39–41°S) have led to a misleading Paleocene-lower Eocene age assignation (see González Bonorino, 1973; González Bonorino and González Bonorino, 1978; González Díaz,1979). In this context, the northern part of the El Maitén Belt is presently described in geological literature as typically Oligocene, with younger ages reaching the lower Miocene (Aragón et al., 2011a; Bechis et al., 2014; Rapela et al., 1988).

As part of the southern extreme of the El Maitén Belt, previous studies on the Rivadavia range determined a middle Eocene age for the interbedded continental sedimentary rocks with fungal spores (Sepúlveda, 1980). Our new U-Pb age of ~37 Ma constraints this sequence to the upper Eocene, which is an unequivocal evidence for an older age for the beginning of the El Maitén Belt magmatism. However, it is worth noting that the dated sample is located in the middle part of the stratigraphic column (Fig. 4), implying that this section of the El Maitén Belt could be even older. Particularly, the probability density functions of detrital zircon ages (Fig. 5) show a ~50 Ma peak that could represent an age closer to the lower terms of this unit or inherited zircons of the Pilcaniyeu Belt.

Our geochemical analyses of the volcanic rocks of the Rivadavia range indicate that they are basic to intermediate lava flows mostly assignable to tholeiitic series (Fig. 6). Their evolution is marked by

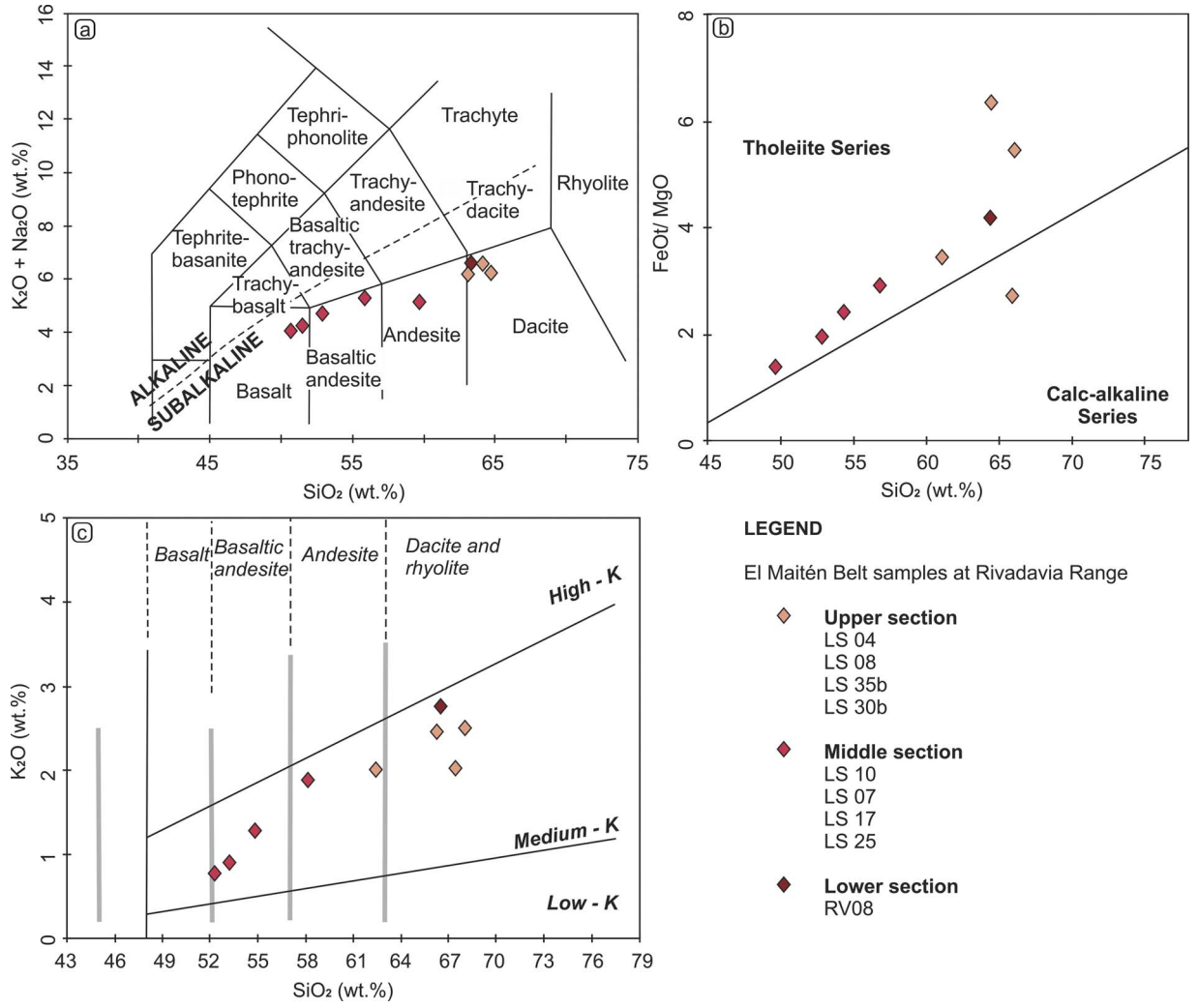

Fig. 6. (a) Total alkali vs. silica classification (TAS). Alkaline and subalkaline fields are according to Irvine and Baragar (1971), (b) FeOt/MgO vs. SiO_2 (Miyashiro, 1974) and (c) K_2O vs. SiO_2 diagrams. K_2O vs. SiO_2 fields are after Le Maitre et al. (2002).

early crystallization stages that involve fractionation of magnesium olivines and later fractionation of clinopyroxene, amphibole, minor calcic plagioclase, ilmenite, titanomagnetite, and apatite (Figs. 7–9). Petrographic, stratigraphic and geochemical analyses through the different facies allowed the discrimination of diverse volcanic pulses. The first pulse included lavas and pyroclastic rocks of more silicic compositions (basaltic andesites and crystalolithic tuffs facies), followed by a second pulse of basic to intermediate lava flows (fine grained basalts, vesicular basalts, volcanic breccias 1, volcanic breccias 2 and aphanitic basalts facies) and a last and more differentiated pulse, unconformably covering previous episodes, composed of dacitic lava flows and associated dykes (columnar andesites facies).

These volcanic rocks have an arc-related signature, shown by trace elements patterns and ratios, with typical LILE and LREE enrichment respect to the HFSE and HREE (Figs. 8 and 10). Discrepancies with arc-like features are given by lower Ba/La, Ba/Ta and Ba/Nb ratios (Fig. 10a and b). Ba/La and Ba/Ta ratios are often associated with the contribution of slab-derived fluids into the mantle wedge, and therefore, these low values would suggest little fluid intake. However, mobile elements composition is comparable with the SSVZ ratios, while Ba content shows to be strongly controlled by amphibole fractionation in more acidic rocks, justifying the lower ratios (Fig. 9). Studied samples have increasing Th/Yb ratios (Th/Yb = 0.6–2.7) against increasing Ta/Yb (Ta/Yb = 0.18–0.29) (Fig. 10d), typically associated with higher contributions of arc components to the magma (Gorton and Schandl, 2000). It is noteworthy that the analyzed samples span the fields of within-plate volcanic zones (WPVZ) and active continental margins (ACM), similarly to the behavior observed in complex regions, where volcanism is transitional between subduction- to extension-related (Gorton and Schandl, 2000; Lipman, 1987). Additionally, Ta/Hf ratios (Ta/Hf = 0.09–0.15) show comparable values to those of arc volcanism (Ta/Hf < 0.15), whereas Th/Hf ratios (Th/Hf = 0.39–1.40) indicate tholeiitic/MORB sources rather than typical calc-alkaline ones (Fig. 10), though the more evolved and younger products show a trend to a more calc-alkaline-like imprint.

The analyzed samples show a tendency to Th enrichment (Th = 1.81–9.25), when compared to U/Th ratio (U/Th = 0.13–0.3), and present a trend toward GLOSS (Global Subducted Sediments) composition (Fig. 10c and e). Some arcs bear high Ba/La and U/Th ratios as a result of slab-derived fluids contributions, while others are characterized by higher Th contents and thus higher Th/Yb ratios, more compatible with sediment recycling (Hawkesworth et al., 1997; Woodhead et al., 2001). Overall, in the analyzed volcanic rocks, the low U/Th ratios, together with the Ba/La and Ba/Ta behavior, would refer to the scarce slab-derived fluids input, despite Ba content being influenced by amphibole fractionation in the more silica-rich samples. However, the increasing Th content trend versus U/Th ratios could reflect sediment supply into the mantle source.

In conjunction, the early stages of El Maitén Belt magmatism, represented by the ~37 Ma volcanic pulses in the Rivadavia range, are

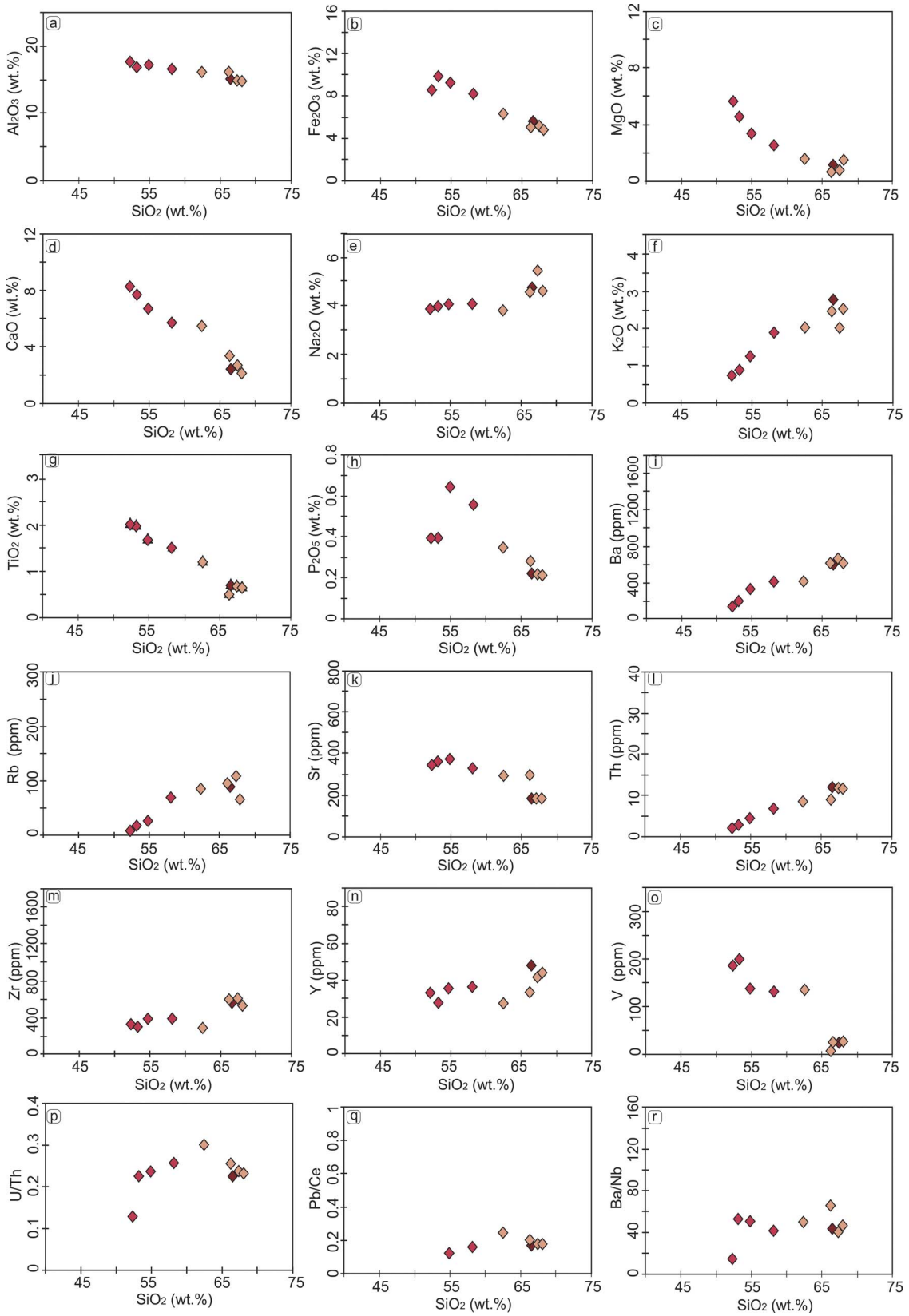

Fig. 7. (a–o) Major, minor and trace elements vs. silica content plots. (p–q) Variation of selected trace elements ratios vs. silica content for El Maitén Belt analyzed volcanic samples. Symbols are as in Fig. 6.

signed by a clear arc signature. However, contrarily to typical arc settings, where fluid-flux melting is the main magma generation process (e.g., Tatsumi, 1989), the genesis of these magmas with tholeiitic sources and limited slab contributions suggests that a different melting process should be operating. The scarce mobile elements input is best explained through the model of decompression melting at shallow

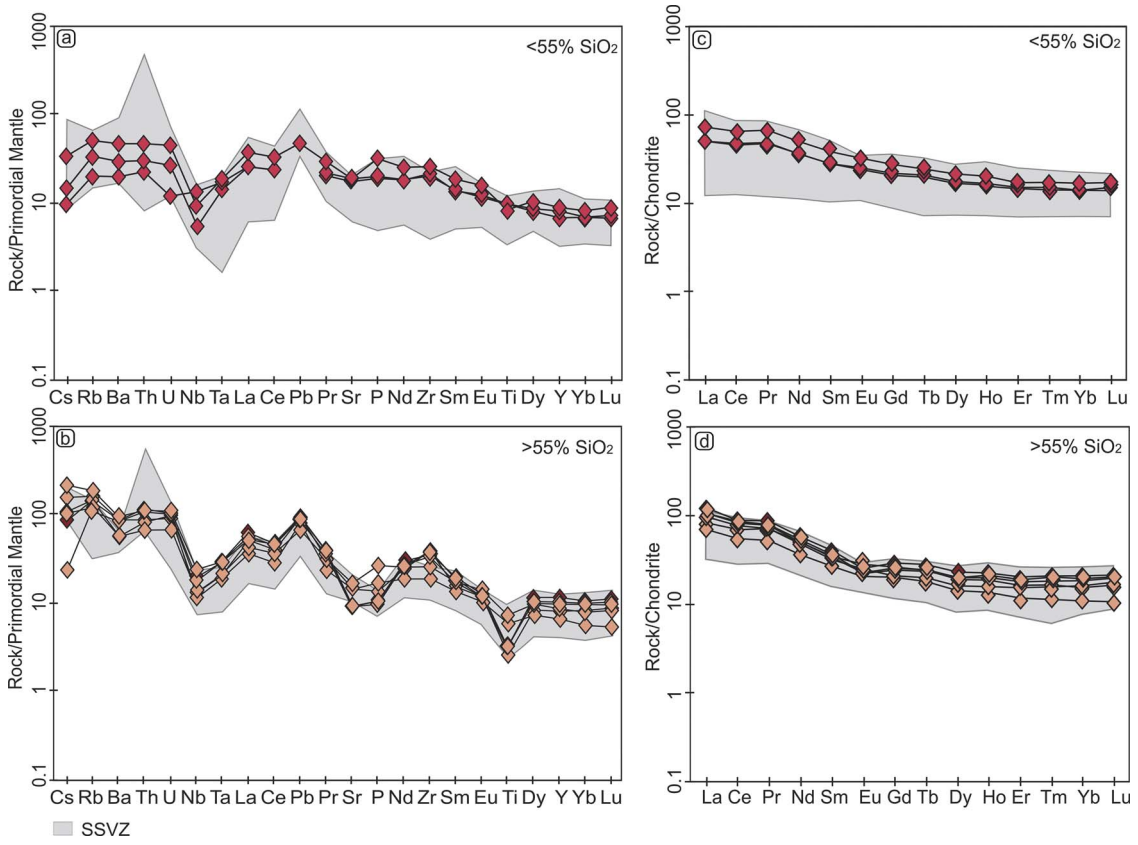

Fig. 8. (a-b) Trace element plots normalized to primitive mantle values (Sun and McDonough, 1989). (c-d) Chondrite-normalized (Nakamura, 1974) spider diagrams for El Maitén Belt samples. Shaded areas correspond to the patterns of the present arc-related volcanic rocks from the SSVZ (Amigo et al., 2013; Lopez-Escobar et al., 1995; Watt et al., 2011). Symbols are as in Fig. 6.

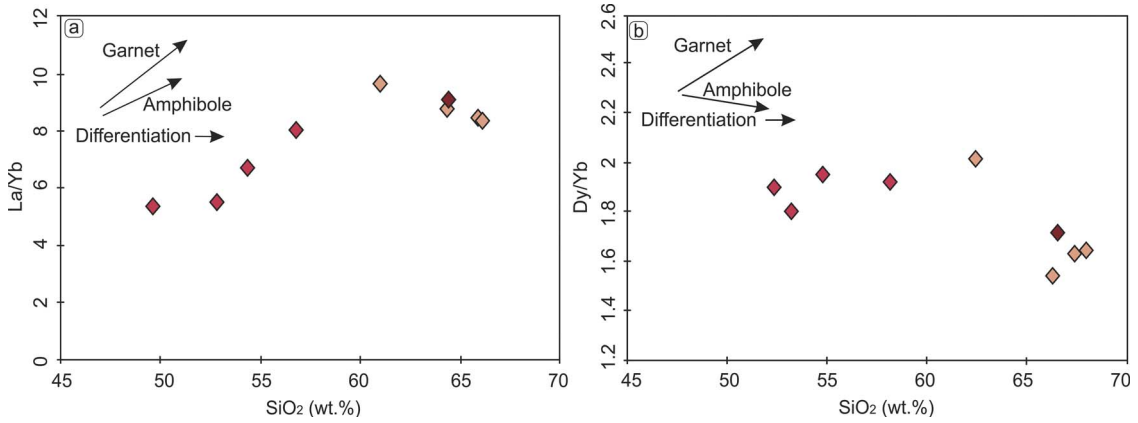

Fig. 9. (a) La/Yb and (b) Dy/Yb ratios versus SiO_2. El Maitén Belt volcanic rocks show increasing La/Yb and decreasing Dy/Yb ratios with increasing silica content, consistent with amphibole fractionation. Symbols are as in Fig. 6.

depths in the mantle wedge (< 70 km), where the effect of fluids and sediment recycling is probably secondary in magma generation (Lee et al., 2009). Despite fluid-flux melting is one of the most common processes by which magma is generated in arc fronts, it was demonstrated that decompression melting also occurs in arc settings (Sisson and Bronto, 1998). Subduction zones dominated by slab flux melting show that slab input (e.g., Ba/La ratio) correlates directly with the degree of melt production (e.g., La/Yb ratio) (e.g., Agostini et al., 2008; Carr et al., 2007; Hochstaedter et al., 1996; Tatsumi, 1989). In this way, Fig. 10f shows that the present-day arc zone at the same latitudes (SSVZ) displays a steep negative trend, supporting fluid-flux melting as the increase in Ba/La ratio raises with decreasing La/Yb. On the contrary, the upper Eocene studied volcanic rocks are characterized by a relatively subordinate slab signature, with almost no correlation between Ba/La and La/Yb (Fig. 10f). This corroborates the prominent role of decompression melting beneath El Maitén Belt, in detriment of fluid-flux contribution from the slab.

Low La/Yb and Dy/Yb ratios for the analyzed samples, regardless their silica content, reflect their equilibrium with low pressure residual mineral assemblages (Fig. 9). As some authors suggest, this could reflect magma equilibration at relatively shallow levels within the crust and/or in a relatively thin crust (Ducea et al., 2015b; Profeta et al., 2015). This is consistent with petrographical characterization where aphyric textures suggest low time of residence within the crust. Moreover, this is supported by decompression melting as the main process in magma generation and by the presence of extensional structures controlling the

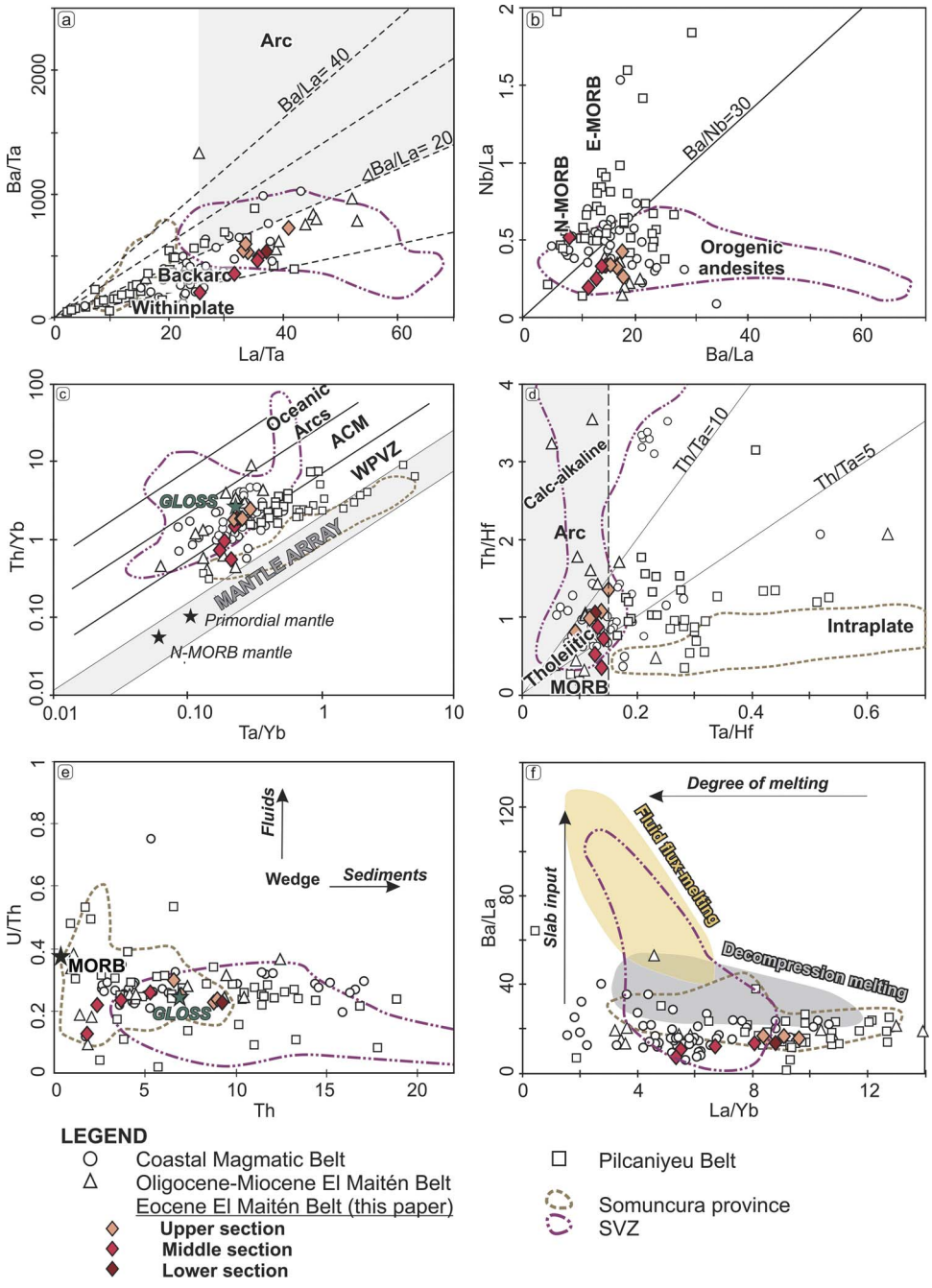

Fig. 10. Plots of (a) Ba/Ta versus La/Ta and (b) Nb/La versus Ba/La. El Maitén Belt samples show La/Ta and Nb/La ratios similar to arc compositions, with lower values for Ba/La, Ba/Ta and Ba/Nb ratios. (c) Th/Yb versus Ta/Yb diagram from Gorton and Schandl (2000; revised after Pearce (1983)) for El Maitén Belt samples showing subduction enrichment trends. ACM is for active continental margins and WPVZ for within-plate volcanic zones. (d) Th/Hf versus Ta/Hf diagram shows that the studied samples respond to tholeiitic arc sources. (e) U/Th versus Th diagram (Hawkesworth et al., 1997). The studied samples show limited slab-fluids input relative to sediment supply. (f) Ba/La versus La/Yb diagram for the investigated samples depicting main melting processes in the mantle wedge.

emplacement of these volcanic sequences. Decompression melting is a typical process in arc-extensional settings, such as occurs in the Central America volcanic front, where the rate of extension controls the degree of melting and facilitates rapid magma ascent (Cameron et al., 2003; Mattioli et al., 2016).

5.2. Implications of late Eocene arc volcanism in the evolution of paleogene–early neogene magmatism at the North Patagonian Andes

In order to evaluate spatiotemporal changes in magmatic activity along the North Patagonian Andes during the Paleogene to Early Neogene, we compared the Eocene rocks of the El Maitén Belt at the Rivadavia range with both older and younger volcanic series in neighbor regions (Fig. 11).

5.2.1. Paleocene–late Eocene

Magmatic activity during the Mesozoic took place in the axial part of the North Patagonian Andes, represented by the North Patagonian Batholith (Aragón et al., 2011a; Castro et al., 2011; González Díaz, 1979; González Díaz and Lizuaín, 1984; Pankhurst et al., 1999) with its volcanic counterparts spread out toward the east (Fig. 2) (Echaurren et al., 2017; Haller and Lapido, 1982). An eastward migration of the arc activity occurred during the Late Cretaceous, with subsequently a waning in arc-related magmatism (Echaurren et al., 2016; Suárez et al., 2010). Meanwhile, volcanic rocks with a within-plate signature occurred in the Pilcaniyeu Belt, in the former retroarc zone (~58–47 Ma; Aragón et al., 2013, 2011b) (Fig. 11d). This volcanism is geochemically characterized by relatively elevated content of HFSE indicating no slab-derived fluids contribution and low percentages of mantle melting (Ba/Ta = 1.84–378.75, La/Ta = 0.36–32.89 and Nb/Yb = 0.42–29.72; Fig. 11a–c). Younger outcrops of the Pilcaniyeu Belt magmatism

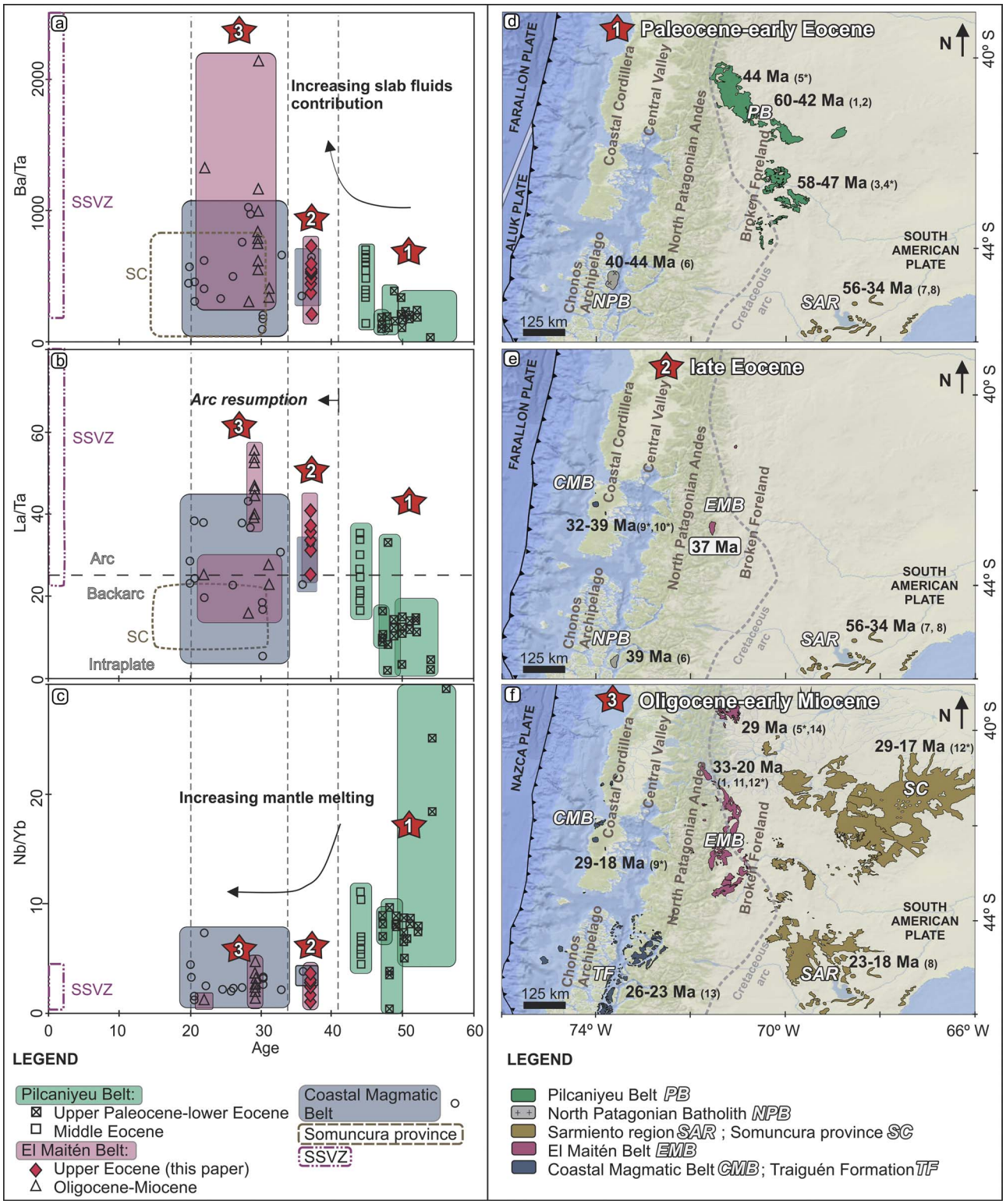

Fig. 11. (a–c) Geochemical diagrams showing arc signature evolution over time: (a) Ba/Ta versus age, (b) La/Ta versus age and (c) Nb/Yb versus age. (d–e) Magmatic units over time: (d) Paleocene-early Eocene, (e) late Eocene, and (f) late Oligocene-early Miocene. Geochemical data of Pilcaniyeu Belt from Aragón et al. (2011b); Oligocene–Miocene El Maitén Belt data from Aragón et al. (2011a), Iannelli et al. (2017b) and Kay et al. (2007); Coastal Magmatic Belt from Henríquez Ascencio (2016), López-Escobar and Vergara (1997) and Muñoz et al. (2000); and present arc data from the SSVZ from Amigo et al. (2013), Lopez-Escobar et al. (1995) and Watt et al. (2011). Geocronological data from: 1) Rapela et al. (1983), 2) González Díaz (1979), 3) Mazzoni et al. (1991) 4) Aragón et al. (2011b), 5) Iannelli et al. (2017b), 6) Pankhurst et al. (1999), 7) Lema and Cortés (1987), 8) Bruni et al. (2008), 9) Muñoz et al. (2000), 10) Henríquez Ascencio (2016), 11) (Rapela et al. (1988), 12) Kay et al. (2007), 13) Encinas et al. (2016), and 14) Ramos et al. (2014).

(~44 Ma), where it gets closer to the Andean axis (Fig. 11d), also show enriched sources and an alkaline-like tendency, although with a more arc-like signature for some trace elements ratios (Iannelli et al., 2017b).

On the contrary, our studies on upper Eocene (~37 Ma) volcanic rocks of the El Maitén Belt, located in the eastern North Patagonian Andes and west of the Pilcaniyeu Belt (Fig. 11e), show unequivocal signals of

slab-derived components with Ba/Ta, La/Ta and Nb/Yb ratios comparable with the present-day magmatic arc (Fig. 11a–c). The contrasting signature of these two Paleogene volcanic episodes implies an evolution from Paleocene-middle Eocene within-plate magmatism in the retroarc zone to a late Eocene arc-like magmatism toward the west in the North Patagonian Andes.

Eocene volcanism was registered also to the west, in the Coastal Cordillera and Central Depression, coeval with the igneous activity in the El Maitén Belt (Fig. 11d and e). Small outcrops of ~39–32 Ma plutonic and volcanic rocks occur along the Coastal Magmatic Belt (Fig. 2) (Henríquez Ascencio, 2016; Muñoz et al., 2000; Vergara et al., 1999), and to the south in the Chonos Archipelago, where Pankhurst et al. (1999) described Eocene (~39–44 Ma) granitoid rocks of the North Patagonian Batholith (Fig. 11d and e). Geochemically, Eocene rocks of the Coastal Magmatic Belt have slab-related characteristics, with similar trace elements behavior as the Rivadavia range volcanic rocks (Fig. 11a–c). This coeval association of arc-related volcanic and plutonic suites on the Pacific coast points out to a double or perhaps an expanded arc configuration at this early stage of arc resumption (late Eocene), after a protracted period of within-plate magmatism (latest Cretaceous-Paleocene). This kind of particular configuration of an expanded arc has been described for early stages of subduction systems subjected to extensional stress conditions. During the early Andean subduction system at northern Chile (26–31°S) in Late Jurassic times, a widespread arc and retroarc volcanism was registered with geochemical variations that resembled those in modern island arcs under extensional conditions (Rossel et al., 2013). Other examples include the trans-Mexican Volcanic Belt, where a double arc configuration is associated with extension affecting central Mexico (e.g., Ferrari et al., 2012).

5.2.2. Late eocene–early Miocene

The upper Eocene magmatic component of the El Maitén Belt and the Coastal Magmatic Belt consisted in relatively small volumes of arc activity (Fig. 11e), in comparison with Oligocene-early Miocene volcanic sequences that developed their main eruptive stages (e.g., Muñoz et al., 2000; Rapela et al., 1988) (Fig. 11f). Geochemically, these Oligocene-early Miocene eruptive stages display an arc-like signature, though they registered a large dispersion in Ba/Ta, La/Ta and Nb/Yb values (Aragón et al., 2011b; Iannelli et al., 2017b; Kay et al., 2007; Muñoz et al., 2000; Rapela et al., 1988) (Figs. 10 and 11). As our data show, late Eocene volcanism from the El Maitén Belt (~37 Ma) is characterized by scarce contributions from the slab, while the Oligocene phase of volcanic activity (~29 Ma) shows a higher intake of slab-derived fluids, a more arc-like tendency and calc-alkaline sources (Iannelli et al., 2017b) (Figs. 10 and 11), typical of more mature arc stages (Brown et al., 1984).

To the east in a foreland position (Fig. 11f), the 29–16.6 Ma volcanic rocks of the Somuncura province (Kay et al., 2007, 2004) present a similar life-span as the arc associations (Coastal Magmatic Belt and El Maitén Belt). Even though this foreland volcanism is characterized by La/Ta and Ta/Hf ratios typical of intra-plate settings (La/Ta = 9.04–19.84 and Ta/Hf = 0.14–1.03; Kay et al., 2007, 2004; Remesal et al., 2012) (Figs. 11–13), its most volumetric magmatic pulse shows higher concentrations of mobile elements, which could imply the presence of subducted components into the mantle source (Ba/Ta = 88.10–713.75, Ba/La = 8.97–40.29; Kay et al., 2007, 2004; Remesal et al., 2012).

Overall, Sr/Y and $(La/Yb)_n$ ratios for Paleogene to Early Neogene volcanism in the North Patagonian Andes (Pilcaniyeu Belt, El Maitén Belt, and Coastal Magmatic Belt) show relatively similar values (Fig. 12). Correlations between Sr/Y and $(La/Yb)_n$ ratios with crustal thickness for intermediate rocks in modern subduction-related magmatic arcs suggest that magmas emplaced over thicker crusts evolved initially at deeper average levels than those of thinner crusts (Chapman et al., 2015; Chiaradia, 2015; Ducea et al., 2015b; Profeta et al., 2015). Despite the fact that quantitative estimates are subjected to large errors,

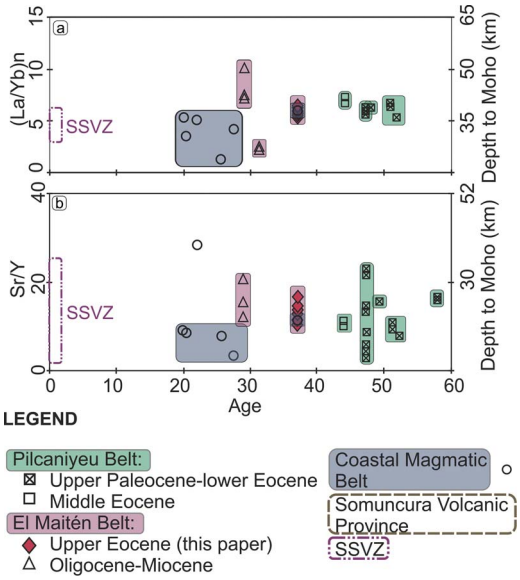

Fig. 12. Chondrite-normalized La/Yb (McDonough and Sun, 1995) and Sr/Y versus time diagram with estimated depths to Moho by Profeta et al. (2015). Normalized La/Yb and Sr/Y for selected samples (see Profeta et al., 2015) show that magmatism was developed within a context of a relatively normal to thin crust.

this method could reflect a qualitative estimation of crustal thickness through time. In this context, Cenozoic crustal thicknesses at the studied latitudes would have remained relatively stable through time, near to 40 km (Fig. 12). However, it is worth highlighting that Oligocene–-Miocene volcanism within the Coastal Magmatic Belt shows relatively lower $(La/Yb)_n$ values, which can be associated with a slightly thinner crust. Despite the restricted data set, the tendency toward lower crustal thicknesses in late Oligocene times is consistent with the mid-Cenozoic extensional conditions proposed in several works. Besides, the association of mafic volcanism with marine deposits of ~22–20 Ma in the El Maitén Belt and in the 26–23 Ma Traiguén Formation constitutes direct evidence of a thinned crust by early Miocene times (Bechis et al., 2014; Encinas et al., 2016, 2014; Litvak et al., 2014; Muñoz et al., 2000) (see Fig. 11f).

5.3. Paleogene tectonic evolution of North Patagonia: late Eocene arc resumption

After a shallow subduction configuration achieved in Late Cretaceous times (Echaurren et al., 2016; Gianni et al., 2015), Paleocene geodynamic reconstructions show the subduction of the Aluk plate beneath the South American plate at low convergence rates (Cande and Leslie, 1986; Somoza and Ghidella, 2005) (Fig. 13a). The tectonic scenario proposed by Aragón et al. (2013, 2011b); indicates that this oblique subduction of the Aluk-Farallón mid-ocean ridge, at about 50–52 Ma beneath North Patagonia, evolved into a transform margin with the interruption of the subduction zone and the arc activity until Miocene times. In that model, the Pilcaniyeu Belt volcanism would have been the result of an asthenospheric upwelling caused by the detachment and sinking of the Aluk plate at depth (Fig. 13) (Aragón et al., 2013). In contrast, Echaurren et al. (2016) interpreted this within-plate volcanism at the Pilcaniyeu Belt as a consequence of the Farallón plate rollback. However, the subduction of the Aluk-Farallón mid-ocean ridge has recently been associated to the north (35°30′S) with Late Cretaceous intraplate volcanism, implying a trend of younger retroarc eruptions to the south in which the Pilcaniyeu Belt magmatic activity could be part, suggesting the possibility of a diachronous opening of an asthenospheric window (Iannelli et al., 2017a).

Beyond the mechanisms associated with the development of the within-plate series, geochronological and geochemical data of the

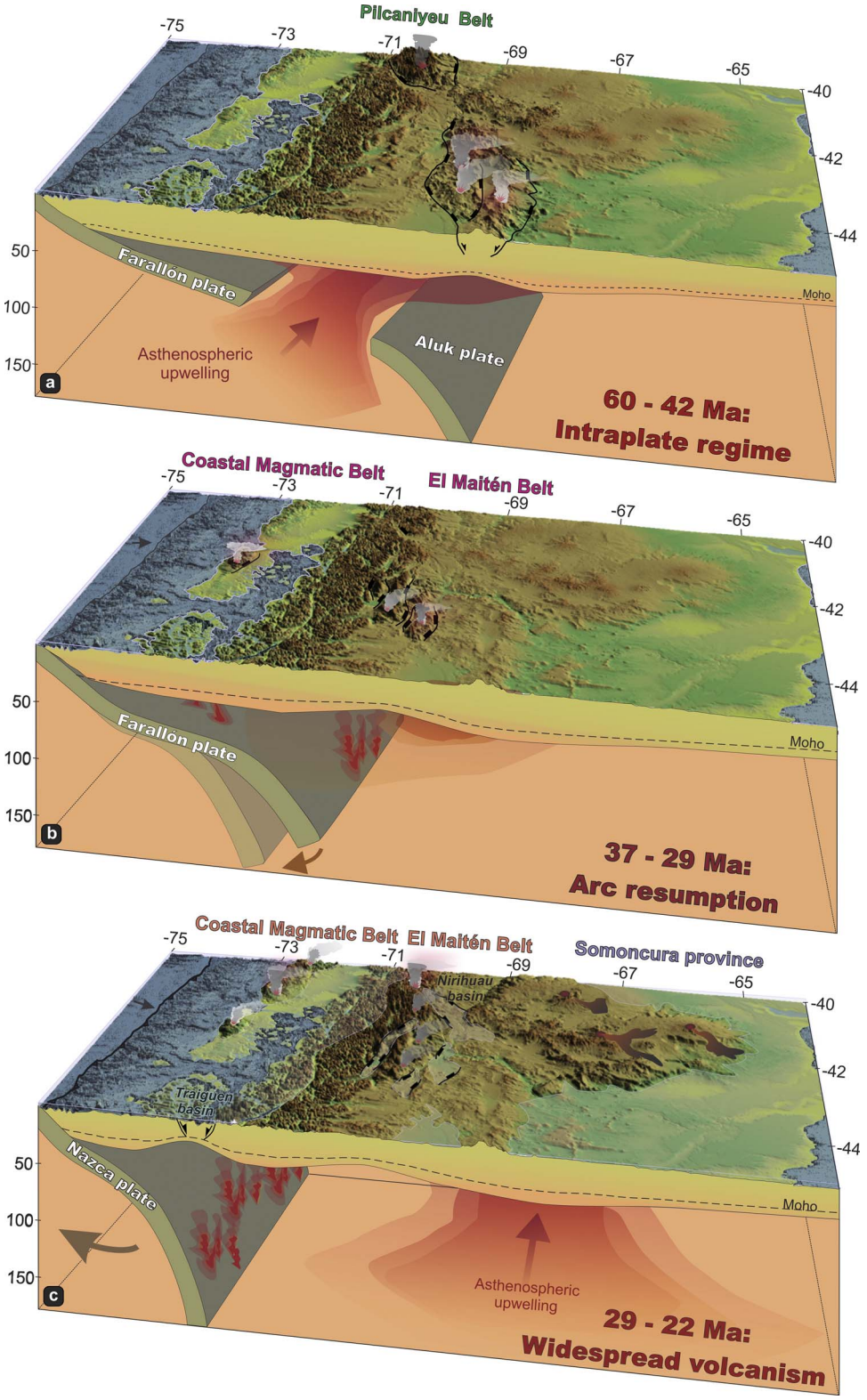

Fig. 13. Late Eocene to early Miocene geodynamic evolution in North Patagonia. (a) 60–42 Ma reconstructions propose the interaction between the Aluk-Farallón mid-ocean ridge with the North Patagonian margin and the subsequent development of an asthenospheric window associated with the eruption of within-plate series. (b) Late Eocene arc resumption in the west at the North Patagonian Andes associated with an extensional regime (our data). (c) 30–20 Ma evolution characterized by the expansion of the arc activity in a widespread extensional setting as a result of slab rollback, before and during the breakup of the Farallón plate into Cocos and Nazca plates (see text for references).

Rivadavia range presented in this study indicates that the onset of the arc-related volcanism in the North Patagonian Andes occurred at ~37 Ma (Fig. 13b), immediately after the end of the within-plate stage of the Pilcaniyeu Belt. These initial stages consisted in low magmatic volumes, controlled by extensional structures and characterized by a tholeiitic composition with limited slab contributions into the mantle wedge, being decompression melting the main process involved in magma genesis. This scenario is similar to that proposed by Lee et al. (2009) for the Cascades Arc, where subduction of the young and presumably hot Juan de Fuca plate beneath North America, dipping ~54°E (e.g., Govers and Meijer, 2001), was associated with dry decompression melting at shallow depths. It is worth highlighting that despite the slab was young and hot, its rheological properties were not the primary control in subduction angle (Long, 2016). In the same way, the southern Central American margin (from Costa Rica to Panama) has also experienced arc development within an oblique subduction

context, where the increase in obliquity implied a change in the asthenospheric flow and a decrease in the amount of fluids reaching the mantle wedge, resulting in a low volume magmatism that shows minor slab-derived fluids contributions (Herrstrom et al., 1995; Hoernle et al., 2008; Rooney et al., 2015). Then, late Eocene arc resumption in North Patagonia, expressed both in the Coastal Cordillera and in the eastern North Patagonian Andes, coincided with a changing geodynamic scenario in which: i) the oblique subduction of the Farallón plate could have conditioned the limited volume of arc magmatism, ii) the relatively young and presumably hot Farallón oceanic plate could have promoted dry decompression melting at shallow depths in the asthenospheric mantle wedge, while its rheological properties are not the main control in slab dip (at least ~30°), and iii) the extensional regime developed in the upper plate probably allowed a rapid ascent and emplacement of these magmas.

This extensional regime controlling late Eocene magma emplacement, correlates with the studies of Charrier et al. (2009, 2002, 1996), which constrained the beginning of the extensional activity in the intra-arc Abanico Basin (Chile-Principal Cordillera) between ~43 and 36 Ma further north (33–36°S), and the intra-arc Traiguén Basin (Chile) at ~32 Ma to the south (45–46°S) (Encinas et al., 2016). We attribute these correlations with a slab rollback mechanism, which promoted extension in the upper plate all through the Southern Andean margin. In this context, the late Eocene extension may represent a transitional stage prior to the breakup of the Farallón plate into the Nazca and Cocos plates after 28–23 Ma (Cande and Leslie, 1986; Lonsdale, 2005), which leads to intensified widespread extension and increasingly higher magmatic volumes erupted in the El Maitén Belt, the Coastal Magmatic Belt and Somuncura province (Henríquez Ascencio, 2016; Iannelli et al., 2017b; Kay et al., 2007; Muñoz et al., 2000; Rapela et al., 1988; Remesal et al., 2012) (Fig. 13c). This Oligocene–early Miocene stage was described all through the Central and Southern Andean margin (Bechis et al., 2014; Charrier et al., 2002, 1996; Encinas et al., 2016; Kay and Kurtz, 1995; among others), where slab rollback process may have been intensified by the increasing convergence rates under a quasi-stationary upper plate, playing a key role in the distribution and emplacement of these volcanic sequences, coeval to the development of fore- and retro-arc basins (e.g., De Ignacio et al., 2001; Jordan et al., 2001; Kay et al., 2007; Kay and Copeland, 2006; Lonsdale, 2005; Muñoz et al., 2000).

6. Conclusions

Outcrops of the El Maitén Belt in North Patagonia, dated in this study in ~37 Ma comprise basaltic and andesitic lavas with interbedded pyroclastic flows, grouped within eight lithological facies that represent three volcanic pulses. Extensional tectonics controlled the emplacement of this volcanic activity as indicated by the occurrence of synextensional strata associated with normal faults.

Trace elements signature indicates that these rocks are subalkaline, mainly tholeiitic arc-related, with scarce slab-derived fluid and sediment contributions. It is inferred that this volcanism was developed in a normal to relatively thin crust, in which the documented extensional regime promoted a rapid magma ascent from primary sources. Main magma generation process was decompression melting at shallow depths in the mantle wedge.

In a regional context, this volcanism is interpreted as the resumption of arc activity within an extensional setting in the late Eocene of North Patagonia, following a period of Paleocene intraplate magmatism and arc quiescence.

Acknowledgments

This work was financially supported by CONICET (grant 11220150100426CO), University of Buenos Aires (grant UBACYT 20020150100166BA), ANPCyT PICT-2012-1490 and Fondecyt1151146. The authors greatly appreciate the corrections made by two anonymous reviewers and the editor, Prof. Artemieva. The authors also acknowledge Eugenio Aragón and Carlos Rapela for fruitful discussion. This is the contribution number 234 of the Instituto de Estudios Andinos Don Pablo Groeber.

Appendix A. Supplementary data

Supplementary data associated with this article can be found, in the online version, at http://dx.doi.org/10.1016/j.jog.2017.11.005.

References

Agostini, S., Ryan, J.G., Tonarini, S., Innocenti, F., 2008. Drying and dying of a subducted slab: coupled Li and B isotope variations in Western Anatolia Cenozoic Volcanism. Earth Planet. Sci. Lett. 272, 139–147. http://dx.doi.org/10.1016/j.epsl.2008.04.032.

Amigo, Á., Lara, L.E., Smith, V.C., 2013. Holocene record of large explosive eruptions from Chaitén and Michinmahuida Volcanoes, Chile. Andean Geol. 40, 227–248. http://dx.doi.org/10.5027/andgeoV40n2-a.

Aragón, E., Castro, A., Díaz-Alvarado, J., Liu, D.Y., 2011a. The North Patagonian batholith at Paso Puyehue (Argentina-Chile). SHRIMP ages and compositional features. J. South Am. Earth Sci. 32, 547–554. http://dx.doi.org/10.1016/j.jsames.2011.02.005.

Aragón, E., D'Eramo, F., Castro, A., Pinotti, L., Brunelli, D., Rabbia, O., Rivalenti, G., Varela, R., Spakman, W., Demartis, M., Cavarozzi, C.E., Aguilera, Y.E., Mazzucchelli, M., Ribot, A., 2011b. Tectono-magmatic response to major convergence changes in the North Patagonian suprasubduction system; the Paleogene subduction-transcurrent plate margin transition. Tectonophysics 509, 218–237. http://dx.doi.org/10.1016/j.tecto.2011.06.012.

Aragón, E., Pinotti, L., D'eramo, F., Castro, A., Rabbia, O., Coniglio, J., Demartis, M., Hernando, I., Cavarozzi, C.E., Aguilera, Y.E., 2013. The Farallon-Aluk ridge collision with South America: implications for the geochemical changes of slab window magmas from fore- to back-arc. Geosci. Front. 4, 377–388. http://dx.doi.org/10.1016/j.gsf.2012.12.004.

Bechis, F., Encinas, A., Concheyro, A., Litvak, V.D., Aguirre-Urreta, B., Ramos, V.A., 2014. New age constraints for the Cenozoic marine transgressions of northwestern Patagonia, Argentina (41°–43°S): paleogeographic and tectonic implications. J. South Am. Earth Sci. 52, 72–93. http://dx.doi.org/10.1016/j.jsames.2014.02.003.

Bilmes, A., D'Elia, L., Franzese, J.R., Veiga, G.D., Hernández, M., 2013. Miocene block uplift and basin formation in the Patagonian foreland: the Gastre Basin, Argentina. Tectonophysics 601, 98–111. http://dx.doi.org/10.1016/j.tecto.2013.05.001.

Brown, G.C., Thorpe, R.S., Webb, P.C., 1984. The geochemical characteristics of granitoids in contrasting arcs and comments on magma sources. J. Geol. Soc. London 141, 413–426. http://dx.doi.org/10.1144/gsjgs.141.3.0413.

Bruni, S., D'Orazio, M., Haller, M.J., Innocenti, F., Manetti, P., Pécskay, Z., Tonarini, S., 2008. Time-evolution of magma sources in a continental back-arc setting: the Cenozoic basalts from Sierra de San Bernardo (Patagonia, Chubut, Argentina). Geol. Mag. 145, 714–732. http://dx.doi.org/10.1017/S0016756808004949.

Cameron, B.I., Walker, J.A., Carr, M.J., Patino, L.C., Matías, O., Feigenson, M.D., 2003. Flux versus decompression melting at stratovolcanoes in southeastern Guatemala. J. Volcanol. Geotherm. Res. 119, 21–50. http://dx.doi.org/10.1016/S0377-0273(02)00304-9.

Caminos, R., Llambías, E.J., 1984. El basamento cristalino. In: Ramos, V.A. (Ed.), IX Congreso Geológico Argentino. Buenos Aires. pp. 37–63.

Cande, S.C., Leslie, R.B., 1986. Late Cenozoic tectonics of the southern Chile trench. Geophys. Res. 91, 471–496.

Carr, M.J., Saginor, I., Alvarado, G.E., Bolge, L.L., Lindsay, F.N., Milidakis, K., Turrin, B.D., Feigenson, M.D., Swisher, C.C., 2007. Element fluxes from the volcanic front of Nicaragua and Costa Rica. Geochem. Geophys. Geosyst. 8. http://dx.doi.org/10.1029/2006GC001396.

Castro, A., Moreno-Ventas, I., Fernández, C., Vujovich, G., Gallastegui, G., Heredia, N., Martino, R.D., Becchio, R., Corretgé, L.G., Díaz-Alvarado, J., Such, P., García-Arias, M., Liu, D.Y., 2011. Petrology and SHRIMP U-Pb zircon geochronology of Cordilleran granitoids of the Bariloche area, Argentina. J. South Am. Earth Sci. 32, 508–530. http://dx.doi.org/10.1016/j.jsames.2011.03.011.

Cazau, L., Mancini, S., Cangini, J., Spalletti, L.A., Chebli, G., 1989. Cuenca De Ñirihuau, In: Cuencas Sedimentarias Argentinas. Instituto Superior de Correlación Geológica, Universidad Nacional de Tucumán San Miguel de Tucumán.

Chang, Z., Vervoort, J.D., McClelland, W.C., Knaack, C., 2006. U-Pb dating of zircon by LA-ICP-MS. Geochem. Geophys. Geosyst. 7, 1–14. http://dx.doi.org/10.1029/2005GC001100.

Chapman, J.B., Ducea, M.N., DeCelles, P.G., Profeta, L., 2015. Tracking changes in crustal thickness during orogenic evolution with Sr/Y: an example from the North American Cordillera. Geology 43, 919–922. http://dx.doi.org/10.1130/G36996.1.

Chapman, J.B., Ducea, M.N., Kapp, P., Gehrels, G.E., DeCelles, P.G., 2017. Spatial and temporal radiogenic isotopic trends of magmatism in Cordilleran orogens. Gondwana Res. 48, 189–204. http://dx.doi.org/10.1016/j.gr.2017.04.019.

Charrier, R., Wyss, A.R., Flynn, J.J., Swisher III, C.C., Norell, M.A., Zapatta, F., McKenna, M.C., Novacek, M.J., 1996. New evidence for late mesozoic-early Cenozoic evolution of the Chilean Andes in the upper Tinguiririca valley (35°S), central Chile. J. South Am. Earth Sci. 9, 393–422. http://dx.doi.org/10.1016/S0895-9811(96)00035-1.

Charrier, R., Baeza, O., Elgueta, S., Flynn, J.J., Gans, P., Kay, S.M., Muñoz, N., Wyss, A.R., Zurita, E., 2002. Evidence for Cenozoic extensional basin development and tectonic

inversion south of the flat-slab segment, southern Central Andes, Chile (33°–36°S.L.). J. South Am. Earth Sci. 15, 117–139. http://dx.doi.org/10.1016/S0895-9811(02)00009-3.
Charrier, R., Farías, M., Maksaev, V., 2009. Evolución tectónica, paleográfica y metalogénica durante el cenozoico en los Andes de Chile norte y central e implicaciones para las regiones adyacentes de Bolivia y Argentina. Rev. la Asoc. Geol. Argent. 65, 5–35.
Chiaradia, M., 2015. Crustal thickness control on Sr/Y signatures of recent arc magmas: an Earth scale perspective. Sci. Rep. 5, 8115. http://dx.doi.org/10.1038/srep08115.
Cole, R.B., Stewart, B.W., 2009. Continental margin volcanism at sites of spreading ridge subduction: examples from southern Alaska and western California. Tectonophysics 464, 118–136. http://dx.doi.org/10.1016/j.tecto.2007.12.005.
Cross, T.A., Pilger, R.H., 1982. Controls of subduction geometry location of magmatic arcs and tectonics of arc and back-arc regions. Geol. Soc. Am. Bull. 93, 545–562. http://dx.doi.org/10.1130/0016-7606(1982)93<545:COSGLO>2.0.CO;2.
Dalla Salla, L., Leguizawjn, M., Mazzoni, M., Rapela, C., Spalletti, L., 1981. Características del vulcanismo paleógeno en la cordillera Nordpatagónica entre las latitudes 39° 30' y 41° 20' S. In: VIII Congreso Geológico Argentino. San Luis. pp. 629–657.
Davidson, J., Turner, S., Handley, H., Macpherson, C., Dosseto, A., 2007. Amphibole sponge in arc crust? Geology 35, 787–790. http://dx.doi.org/10.1130/G23637A.1.
De Ignacio, C., López, I., Oyarzún, R., Márquez, A., 2001. The northern Patagonia Somuncura plateau basalts: a product of slab-induced, shallow asthenospheric upwelling? Terra Nov. 13, 117–121.
DeCelles, P.G., Ducea, M.N., Kapp, P., Zandt, G., 2009. Cyclicity in Cordilleran orogenic systems. Nat. Geosci. 2, 251–257. http://dx.doi.org/10.1038/ngeo469.
Dickinson, W.R., Gehrels, G.E., 2003. U-Pb ages of detrital zircons from Permian and Jurassic eolian sandstones of the Colorado Plateau, USA: paleogeographic implications. Sediment. Geol. 163, 29–66. http://dx.doi.org/10.1016/S0037-0738(03)00158-1.
Ducea, M.N., Paterson, S.R., DeCelles, P.G., 2015a. High-volume magmatic events in subduction systems. Elements 11, 99–104. http://dx.doi.org/10.2113/gselements.11.2.99.
Ducea, M.N., Saleeby, J.B., Bergantz, G., 2015b. The architecture, chemistry, and evolution of continental magmatic arcs. Annu. Rev. Earth Planet. Sci. 43, 299–333. http://dx.doi.org/10.1146/annurev-earth-060614-105049.
Echaurren, A., Folguera, A., Gianni, G., Orts, D., Tassara, A., Encinas, A., Giménez, M., Valencia, V., 2016. Tectonic evolution of the North Patagonian Andes (41°–44°S) through recognition of syntectonic strata. Tectonophysics 677, 99–114. http://dx.doi.org/10.1016/j.tecto.2016.04.00.
Echaurren, A., Oliveros, V., Folguera, A., Ibarra, F., Creixell, C., Lucassen, F., 2017. Early Andean tectonomagmatic stages in north Patagonia: insights from field and geochemical data. J. Geol. Soc. London 174 (3), 405–421. http://dx.doi.org/10.1144/jgs2016-087.
Encinas, A., Pérez, F., Nielsen, S.N., Finger, K.L., Valencia, V., Duhart, P., 2014. Geochronologic and paleontologic evidence for a pacific-atlantic connection during the late oligocene-early miocene in the patagonian andes (43–44°S). J. South Am. Earth Sci. 55, 1–18. http://dx.doi.org/10.1016/j.jsames.2014.06.008.
Encinas, A., Folguera, A., Oliveros, V., De Girolamo Del Mauro, L., Tapia, F., Riffo, R., Hervé, F., Finger, K.L., Valencia, V.A., Gianni, G., 2016. Late Oligocene–early Miocene submarine volcanism and deep-marine sedimentation in an extensional basin of southern Chile: implications for the tectonic development of the North Patagonian Andes. Geol. Soc. Am. Bull. 128, 807–823. http://dx.doi.org/10.1130/B31303.1.
Ferrari, L., Orozco-Esquivel, T., Manea, V., Manea, M., 2012. The dynamic history of the Trans-Mexican Volcanic Belt and the Mexico subduction zone. Tectonophysics 522–523, 122–149. http://dx.doi.org/10.1016/j.tecto.2011.09.018.
Feruglio, E., 1949. Descripcion geológica de la Patagonia, Direccion general de Yacimientos Petroliferos Fiscales. Editorial Coni, Buenos Aires.
Folguera, A., Ramos, V.A., 2011. Repeated eastward shifts of arc magmatism in the Southern Andes: a revision to the long-term pattern of Andean uplift and magmatism. J. South Am. Earth Sci. 32, 531–546. http://dx.doi.org/10.1016/j.jsames.2011.04.003.
Giacosa, R.E., Afonso, J.C., Nemesio Heredia, C., Paredes, J., 2005. Tertiary tectonics of the sub-Andean region of the North Patagonian Andes, southern central Andes of Argentina (41–42°30'S). J. South Am. Earth Sci. 20, 157–170. http://dx.doi.org/10.1016/j.jsames.2005.05.013.
Gianni, G., Navarrete, C., Orts, D., Tobal, J., Folguera, A., Giménez, M., 2015. Patagonian broken foreland and related synorogenic rifting: the origin of the Chubut Group Basin. Tectonophysics 649, 81–99. http://dx.doi.org/10.1016/j.tecto.2015.03.006.
Gill, J.B., 1981. Orogenic Andesites and Plate Tectonics, Minerals and Rocks. Springer, Berlin Heidelberg, Berlin, Heidelberg. http://dx.doi.org/10.1007/978-3-642-68012-0.
González Bonorino, F., González Bonorino, G., 1978. Geología de la region de San Carlos de Bariloche. Rev. la Asoc. Geol. Argent. 33, 175–210.
González Bonorino, F., 1973. Geología del área entre San Carlos de Bariloche y Llao Llao. Fundacion Bariloche, Departamento de Recursos Naturales y Energía.
González Díaz, E.F., Lizuaín, A., 1984. El Complejo Volcano-clástico y plutónico del sector cordillerano. In: Ramos, V.A. (Ed.), IX Congreso Geológico Argentino, Relatorio 5. San Carlos de Bariloche. pp. 119–138.
González Díaz, E.F., 1979. La edad de la Formacion Ventana, en el área al norte y al este del lago Nahuel Huapi. Rev. la Asoc. Geol. Argent. 34, 113–124.
González, P., 1994. Mapa Geológico de la Provincia de Río Negro. República Argentina. Escala 1:750.000. Secr. Minería, Dir. Nac. del Serv. Geológico.
Gordon, A., Ort, M.H., 1993. Edad y correlación del plutonismo subcordillerano en las provincias de Río Negro y Chubut (41–42° 30'LS). In: VII Congreso Geológico Argentino. Mendoza. pp. 120–127.
Gorton, M.P., Schandl, E.V.A.S., 2000. From continents to island arcs: a geochemical index of tectonic setting for arc-related and within-plate felsic to intermediate volcanic rocks. Can. Mineral. 38, 1065–1073.
Govers, R., Meijer, P.T., 2001. On the dynamics of the Juan de Fuca plate. Earth Planet. Sci. Lett. 189, 115–131. http://dx.doi.org/10.1016/S0012-821X(01)00360-0.
Haller, M.J., Lapido, O.R., 1982. The Jurassic-Cretaceous volcanism in the Septentrional Patagonian Andes. Earth Sci. Rev. 18, 395–410. http://dx.doi.org/10.1016/0012-8252(82)90046-0.
Hawkesworth, C.J., Turner, S.P., McDermott, F., Peate, D.W., van Calsteren, P., 1997. U-Th isotopes in arc magmas: implications for element transfer from the subducted crust. Science 276 (80-), 551–555. http://dx.doi.org/10.1126/science.276.5312.551.
Henríquez Ascencio, G.J., 2016. Petrografía, geoquímica y marco geotectónico del Complejo Volcánico Ancud, Provincia de Chiloé, Región de los Lagos, Chile. Universidad de Concepción.
Herrstrom, E.A., Reagan, M.K., Morris, J.D., 1995. Variations in lava composition associated with flow of asthenosphere beneath southern Central America. Geology 23, 617–620. http://dx.doi.org/10.1130/0091-7613(1995)023<0617:VILCAW>2.3.CO;2.
Hervé, F., Pankhurst, R.J., Drake, R., Beck, M.E., 1995. Pillow metabasalts in a mid-Tertiary extensional basin adjacent to the Liquiñe-Ofqui fault zone: the Isla Magdalena area Aysén, Chile. J. South Am. Earth Sci. 8, 33–46.
Heuret, A., Lallemand, S., 2005. Plate motions, slab dynamics and back-arc deformation. Phys. Earth Planet. Inter. 149, 31–51. http://dx.doi.org/10.1016/j.pepi.2004.08.022.
Hochstaedter, A.G., Ryan, J.G., Luhr, J.F., Hasenaka, T., 1996. On B/Be ratios in the Mexican Volcanic Belt. Geochim. Cosmochim. Acta 60, 613–628. http://dx.doi.org/10.1016/0016-7037(95)00415-7.
Hoernle, K., Abt, D.L., Fischer, K.M., Nichols, H., Hauff, F., Abers, G.A., van den Bogaard, P., Heydolph, K., Alvarado, G., Protti, M., Strauch, W., 2008. Arc-parallel flow in the mantle wedge beneath Costa Rica and Nicaragua. Nature 451, 1094–1097. http://dx.doi.org/10.1038/nature06550.
Hofmann, A.W., Jochum, K.P., Seufert, M., White, W.M., 1986. Nb and Pb in oceanic basalts: new constraints on mantle evolution. Earth Planet. Sci. Lett. 79, 33–45. http://dx.doi.org/10.1016/0012-821X(86)90038-5.
Horton, B.K., Fuentes, F., 2016. Sedimentary record of plate coupling and decoupling during growth of the Andes. Geology 44, 647–650. http://dx.doi.org/10.1130/G37918.1.
Iannelli, S.B., Fennell, L.M., Litvak, V.D., Fernández Paz, L., Folguera, A., 2017a. Volcanismo Cretácico Superior-Paleoceno en la alta cordillera al sur de la Provincia de Mendoza (35°30'). In: XX Congreso Geológico Argentino. Tucumán. pp. 138–139.
Iannelli, S.B., Litvak, V.D., Fernández Paz, L., Folguera, A., Ramos, M.E., Ramos, V.A., 2017b. Evolution of Eocene to Oligocene arc-related volcanism in the North Patagonian Andes (39–41S), prior to the break-up of the Farallon plate. Tectonophysics 696–697, 70–87. http://dx.doi.org/10.1016/j.tecto.2016.12.024.
Irvine, T.N., Baragar, W.R.A., 1971. A guide to the chemical classification of the common volcanic rocks. Can. J. Earth Sci. 8, 523–548. http://dx.doi.org/10.1139/e71-055.
Jacques, G., Hoernle, K., Gill, J., Hauff, F., Wehrmann, H., Garbe-Schönberg, D., van den Bogaard, P., Bindeman, I., Lara, L.E., 2013. Across-arc geochemical variations in the Southern Volcanic Zone, Chile (34. 5–38.0°S): constraints on mantle wedge and slab input compositions. Geochim. Cosmochim. Acta 123, 218–243. http://dx.doi.org/10.1016/j.gca.2013.05.016.
Jordan, T.E., Burns, W.M., Veiga, R., Pángaro, F., Copeland, P., Kelley, S., Mpodozis, C., 2001. Extension and basin formation in the southern Andes caused by increased convergence rate: a mid-Cenozoic trigger for the Andes. Tectonics 20, 308–324.
Karlstrom, L., Lee, C.A., Manga, M., 2014. The role ofmagmatically driven lithospheric thickening on arc front migration. Geochem. Geophys. Geosyst. 15, 2655–2675. http://dx.doi.org/10.1002/2014GC005355.
Kay, S.M., Copeland, P., 2006. Early to middle Miocene backarc magmas of the Neuquén Basin: geochemical consequences of slab shallowing and the westward drift of South America. Geol. Soc. Am. Spec. Pap. 407, 185–213. http://dx.doi.org/10.1130/2006.2407(09).
Kay, S.M., Kurtz, A., 1995. Magmatic and tectonic characterization of the El Teniente region, Unpublished report. CODELCO.
Kay, S.M., Gorring, M., Ramos, V.A., 2004. Magmatic sources, setting and causes of tertiary to recent patagonian plateau magmatism (36°S–52°S latitude). Rev. la Asoc. Geol. Argent. 59, 556–568.
Kay, S.M., Ardolino, A.A., Gorring, M.L., Ramos, V.A., 2007. The Somuncura Large Igneous Province in Patagonia: interaction of a transient mantle thermal anomaly with a subducting slab. J. Petrol. 48, 43–77. http://dx.doi.org/10.1093/petrology/egl053.
López-Escobar, L., Vergara, M., 1997. Eocene-Miocene longitudinal depression and Quaternary volcanism in the Southern Andes, Chile (33–42.5°S): a geochemical comparison. Rev. Geol. Chile 24, 227–244.
Lavenu, A., Cembrano, J., 1999. Compressional and transpressional stress pattern for the Pliocene and Quaternary (Andes of central and southern Chile). J. Struct. Geol. 21, 1669–1691. http://dx.doi.org/10.1016/S0191-8141(99)00111-X.
Le Maitre, R.W., Streckeisen, A., Zanettin, B., Le Bas, M.J., Bonin, B., Bateman, P., Bellieni, G., Dudek, A., Efremova, S., Keller, J., 2002. Igneous rocks: a classification and glossary of terms: recommendations of the International Union of Geological Sciences. Subcommission on the Systematics of Igneous Rocks. Cambridge University Press.
Lee, C.T.A., Luffi, P., Plank, T., Dalton, H., Leeman, W.P., 2009. Constraints on the depths and temperatures of basaltic magma generation on Earth and other terrestrial planets using new thermobarometers for mafic magmas. Earth Planet. Sci. Lett. 279, 20–33. http://dx.doi.org/10.1016/j.epsl.2008.12.020.
Lema, H.A., Cortés, J.M., 1987. El vulcanismo eoceno del flanco oriental de la Meseta del

Canquel, Chubut, Argentina. X Congreso Geológico Argentino Actas 188–191.
Lipman, P.W., 1987. Rare-earth-element compositions of Cenozoic volcanic rocks in the southern Rocky Mountains and adjacent areas. In: U.S. Geological Survet Bulletin 1668. Denver.
Litvak, V.D., Encinas, A., Oliveros, V., Bechis, F., Folguera, A., Ramos, V.A., 2014. El volcanismo mioceno inferior vinculado a las ingresiones marinas en los Andes Nordpatagónicos. XIX Congr. Geológico Argentino 1–2.
Lizuain, A., Viera, R.M., 2010. Descripción geológica de la Hoja 4372-I y II, Esquel, Provincia de Chubut. Inst. Geol. y Recur. Miner. Serv. Geol. Min. Argentino. Bol. 369, 1–92.
Lizuain, A., Ragona, D., Folguera, A., 1995. Mapa geológico de la provincia del Chubut, escala 1: 750.000. Secr. Minería Dir. Nac. del Serv. Geol.
Long, M.D., 2016. The Cascadia Paradox: mantle flow and slab fragmentation in the Cascadia subduction system. J. Geodyn. 102, 151–170. http://dx.doi.org/10.1016/j.jog.2016.09.006.
Lonsdale, P., 2005. Creation of the Cocos and Nazca plates by fission of the Farallon plate. Tectonophysics 404, 237–264. http://dx.doi.org/10.1016/j.tecto.2005.05.011.
Lopez-Escobar, L., Cembrano, J., Moreno, H., 1995. Geochemistry and tectonics of the Chilean southern Andes basaltic Quaternary volcanism (37–46°S). Rev. Geol. Chile 22, 219–234. http://dx.doi.org/10.5027/andgeoV22n2-a06.
Ludwig, K.R., 2003. User's manual for Isoplot 3.00: a geochronological toolkit for Microsoft Excel. Kenneth R. Ludwig.
Macpherson, C.G., Dreher, S.T., Thirlwall, M.F., 2006. Adakites without slab melting: high pressure differentiation of island arc magma, Mindanao, the Philippines. Earth Planet. Sci. Lett. 243, 581–593. http://dx.doi.org/10.1016/j.epsl.2005.12.034.
Mattioli, M., Renzulli, A., Agostini, S., Lucidi, R., 2016. Magmas with slab fluid and decompression melting signatures coexisting in the Gulf of Fonseca: evidence from Isla El Tigre volcano (Honduras, Central America). Lithos 240–243, 1–15. http://dx.doi.org/10.1016/j.lithos.2015.10.019.
Mazzoni, M.M., Kawashita, K., Harrison, S., Aragón, E., 1991. Edades radimétricas eocenas, borde occidental de Macizo Norpatagónico. Rev. la Asoc. Geol. Argent. 46, 150–158.
McDonough, W.F., Sun, S. s., 1995. The composition of the Earth. Chem. Geol. 120, 223–253. http://dx.doi.org/10.1016/0009-2541(94)00140-4.
Miyashiro, A., 1974. Volcanic rock series in island arcs and active continental margins. Am. J. Sci. 274, 321–355.
Muñoz, J., Troncoso, R., Duhart, P., Crignola, P., Farmer, L., Stern, C.R., 2000. The relation of the mid-tertiary coastal magmatic belt in south-central Chile to the late Oligocene increase in plate convergence rate. Rev. Geol. Chile 27, 177–203. http://dx.doi.org/10.4067/S0716-02082000000200003.
Nakamura, N., 1974. Determination of REE, Ba, Fe, Mg, Na and K in carbonaceous and ordinary chondrites. Geochim. Cosmochim. Acta 38, 757–775. http://dx.doi.org/10.1016/0016-7037(74)90149-5.
Orts, D.L., Folguera, A., Encinas, A., Ramos, M., Tobal, J., Ramos, V.A., 2012. Tectonic development of the North Patagonian Andes and their related Miocene foreland basin (41°30'–43°S). Tectonics 31, 1–24. http://dx.doi.org/10.1029/2011TC003084.
Paces, J.B., Miller, J.D., 1993. Precise U-Pb ages of Duluth Complex and related mafic intrusions, northeastern Minnesota: geochronological insights to physical, petrogenetic, paleomagnetic, and tectonomagmatic processes associated with the 1.1 Ga Midcontinent Rift System. J. Geophys. Res. Solid Earth 98, 13997–14013. http://dx.doi.org/10.1029/93JB01159.
Pankhurst, R.J., Weaver, S.D., Hervé, F., Larrondo, P., 1999. Mesozoic Cenozoic evolution of the North Patagonian Batholith in Aysén, southern Chile. J. Geol. Soc. London 156, 673–694. http://dx.doi.org/10.1144/gsjgs.156.4.0673.
Pearce, J.A., 1983. Role of the sub-continental lithosphere in magma genesis at active continental margins.
Profeta, L., Ducea, M.N., Chapman, J.B., Paterson, S.R., Gonzales, S.M.H., Kirsch, M., Petrescu, L., DeCelles, P.G., 2015. Quantifying crustal thickness over time in magmatic arcs. Sci. Rep. 5http://dx.doi.org/10.1038/srep17786. Manuscript number: 17786.
Rabassa, J., 1974. Geología superficial en la región de Pilcaniyeu-Comallo, provincia de Río Negro (Unpublished doctoral thesis). Universidad Nacional de La Plata.
Rabassa, J., 1978. Estratigrafía de la región Pilcaniyeu-Comallo, provincia de Río Negro. 7◦ Congreso Geológico Argentino, Actas. pp. 731–746.
Ramos, M.E., Folguera, A., Fennell, L., Giménez, M., Litvak, V.D., Dzierma, Y., Ramos, V.A., 2014. Tectonic evolution of the North Patagonian Andes from field and gravity data (39–40°S). J. South Am. Earth Sci. 51, 59–75. http://dx.doi.org/10.1016/j.jsames.2013.12.010.
Ramos, V.A., 1982. Las ingresiones pacíficas del terciario en el norte de la Patagonia (Argentina). In: III Congreso Geológico Chileno. Concepción. pp. 262–288.
Rapela, C.W., Spalletti, L.A., Merodio, J.C., 1983. Evolución magmática y geotectónica de la Serie Andesítica andina (Paleoceno-Eoceno) en la cordillera Nordpatagónica. Rev. la Asoc. Geol. Argent. 38, 469–484.
Rapela, C.W., Spalletti, L.A., Merodio, J.C., Aragón, E., 1984. El vulcanismo paleoceno-eoceno de la provincia volcánica andino-patagónica. In: IX Congreso Geológico Argentino. San Carlos de Bariloche. pp. 189–213.
Rapela, C.W., Spalletti, L.A., Merodio, J.C., Aragón, E., 1988. Temporal evolution and spatial variation of early tertiary volcanism in the Patagonian Andes (40°S–42°30°S). J. South Am. Earth Sci. 1, 75–88. http://dx.doi.org/10.1016/0895-9811(88)90017-X.
Rapela, C.W., Pankhurst, R.J., Fanning, C.M., Herve, F., 2005. Pacific subduction coeval with the Karoo mantle plume: the early Jurassic subcordilleran belt of northwestern Patagonia. Geol. Soc. 217–239. http://dx.doi.org/10.1144/GSL.SP.2005.246.01.07.
Remesal, M.B., Salani, F.E., Cerredo, M.E., 2012. Petrología del complejo volcánico Barril Niyeu (Mioceno inferior), Patagonia Argentina. Rev. Mex. Ciencias Geol. 29, 463–477.
Rooney, T.O., Morell, K.D., Hidalgo, P., Fraceschi, P., 2015. Magmatic consequences of the transition from orthogonal to oblique subduction in Panama. Geochem. Geophys. Geosyst. 16, 4178–4208. http://dx.doi.org/10.1002/2015GC006150.
Rosenbaum, G., Lister, G.S., 2004. Neogene and Quaternary rollback evolution of the Tyrrhenian Sea, the Apennines, and the Sicilian Maghrebides. Tectonics 23, 1–17. http://dx.doi.org/10.1029/2003TC001518.
Rossel, P., Oliveros, V., Ducea, M.N., Charrier, R., Scaillet, S., Retamal, L., Figueroa, O., 2013. The early Andean subduction system as an analog to island arcs: evidence from across-arc geochemical variations in northern Chile. Lithos 179, 211–230. http://dx.doi.org/10.1016/j.lithos.2013.08.014.
Rubatto, D., 2002. Zircon trace element geochemistry: Partitioning with garnet and the link between U-Pb ages and metamorphism. Chem. Geol. 184, 123–138. http://dx.doi.org/10.1016/S0009-2541(01)00355-2.
Sepúlveda, E.G., 1980. Estudio palinológico de sedimentitas intercaladas en la Serie Andesitica Andina", cordón oriental del Futalaufquen Chubut. Parte I: Restos de hongos. Rev. la Asoc. Geol. Argent. 35, 248–272.
Sernageomin, 2003. Mapa Geológico de Chile: versión digital. Publicación Geológica Digital 4, pp. 25.
Silva, C., 2003. Ambiente geotectónico de erupción y metamorfismo de metabasaltos almohadillados de los Andes Norpatagónicos (42°–46°S), Chile. Universidad de Chile.
Silver, P.G., 1998. Coupling of South American and African plate motion and plate deformation. Science 279 (80-), 60–63. http://dx.doi.org/10.1126/science.279.5347.60.
Sisson, T.W., Bronto, S., 1998. Evidence for pressure-release melting beneath magmatic arcs from basalt at Galunggung, Indonesia. Nature 391, 883–886. http://dx.doi.org/10.1038/36087.
Somoza, R., Ghidella, M.E., 2005. Convergencia en el margen occidental de América del sur durante el Cenozoico: subducción de las placas de Nazca, Farallón y Aluk. Rev. la Asoc. Geol. Argent. 60, 797–809. http://dx.doi.org/10.3989/scimar.2002.66n4433.
Spalletti, L.A., 1983. Paleogeografía de la Formación Ñirihuau y sus equivalentes en la región occidental de Neuquén, Río Negro y Chubut. Rev. la Asoc. Geol. Argent. 38, 454–468.
Suárez, M., De La Cruz, R., Bell, M., Demant, A., 2010. Cretaceous slab segmentation in southwestern Gondwana. Geol. Mag. 147, 193. http://dx.doi.org/10.1017/S0016756809990355.
Sun, S., McDonough, W.F., 1989. Chemical and isotopic systematics of oceanic basalts: implications for mantle composition and processes. Geol. Soc. London Spec. Publ. 42, 313–345. http://dx.doi.org/10.1144/GSL.SP.1989.042.01.19.
Tatsumi, Y., 1989. Migration of fluid phases and genesis of basalt magmas in subduction zones. J. Geophys. Res. 94, 4697–4707.
Turner, J.C., 1982. Descripción geológica de la hoja 44c, Tecka, provincia del Chubut. Serv. Geol. Nac. Bol. 180, 1–92.
Vergara, M., Morata, D., Hickey-Vargas, R., Lopez-Escobar, L., Beccar, I., 1999. Cenozoic tholeiitic volcanism in the Colbún area, Linares precordillera, central Chile (35°35'–36°S). Rev. Geol. Chile 26, 23–41.
Viera, R.L.M., Hughes, G., 1999. El yacimiento polimetálico aurífero Huemules, Chubut. Recur. Miner. la República Argent. 35, 1369–1376.
Volkheimer, W., 1964. Estratigrafía de la zona extraandina del departamento de Cushamen (Chubut) entre los paralelos 42° y los 42°30'y los meridianos 70° y 71°. Rev. la Asoc. Geol. Argent. 19, 85–107.
Vukadinovic, D., 1993. Are Sr enrichments in arc basalts due to plagioclase accumulation? Geology 21, 611–614. http://dx.doi.org/10.1130/0091-7613(1993)021<0611:ASEIAB>2.3.CO.
Watt, S.F.L., Pyle, D.M., Mather, T.A., 2011. Geology, petrology and geochemistry of the dome complex of Huequi volcano southern Chile. Andean Geol. 38, 335–348.
Wehrmann, H., Hoernle, K., Jacques, G., Garbe-Schönberg, D., Schumann, K., Mahlke, J., Lara, L.E., 2014. Volatile (sulphur and chlorine), major, and trace element geochemistry of mafic to intermediate tephras from the Chilean Southern Volcanic Zone (33–43°S). Int. J. Earth Sci. 103, 1945–1962. http://dx.doi.org/10.1007/s00531-014-1006-9.
Woodhead, J.D., Hergt, J.M., Davidson, J.P., Eggins, S.M., 2001. Hafnium isotope evidence for "conservative" element mobility during subduction zone processes. Earth Planet. Sci. Lett. 192, 331–346. http://dx.doi.org/10.1016/S0012-821X(01)00453-8.
Yrigoyen, M.T., 1969. Problemas estratigráficos del Terciario de Argentina. Ameghiniana 6, 315–329.